

UNIVERSITY OF BERGEN



Geophysical Institute

Faculty of Mathematics and Natural Sciences

MASTERS THESIS

**Design of a
Generator Excitation System**

Author: Jonas Fotland Fænn

June 1, 2021

Abstract

The world requires more and more energy, and the synchronous generator is one of the most widely used machine to create electricity. With all the debate about climate changes, and electrification of the power industry, it is therefore important to get a deep comprehension of how the machine works, and how to get the machine to work in reliable conditions. The excitation system provides many features such as simplicity of control, stability and reliability under all conditions. A fully working excitation system is with other words essential to get a reliable power system. This thesis will take a look at the theory surrounding the excitation system, all from the synchronous machine itself, the power electronics and the excitation system. The thesis focus on designing an excitation system for a synchronous machine using Matlab[®]/Simulink[®]. The machine is suppose to be as similar as possible to the Terco MV1027-235 synchronous machine stationed at Western Norway University of Applied Sciences.

The work resulted in a working excitation system based on an single-phase thyristor rectifier. Along with that two control systems were made, one which the field voltage could be manually adjusted, and one which would automatically control the terminal voltage output of the synchronous machine.

Acknowledgment

This master thesis is written in collaboration of the University of Bergen and Western Norway University of Applied Sciences. It marks the end of my two year master study, and a total of five year studying electrical engineering.

I would like to thank my supervisor, Associate professor Emil Cimpan, for great help and guidance during this year. I would also like to thank my co-supervisor Mostafa Paskyabi for help with the report, and at last my three fellow friends; Gabriel Abildgaard, Marius Reigstad and Fredrik Storebø for all discussions and help throughout this five year period.

(JF)

Contents

Abstract	ii
Acknowledgment	iv
List of Figures	vii
List of Tables	x
Acronyms	xi
Symbols	xii
1 Introduction	1
1.1 Literature review	2
1.2 Objective	2
1.3 Structure	3
2 State of the art	4
2.1 SM Theory	4
2.1.1 Construction	5
2.1.2 Voltage Generation	6
2.1.3 Park Transformation	9
2.2 Excitation System	11
2.2.1 Type DC	12
2.2.2 Type AC	12
Stationary rectifiers	13
Rotating rectifiers	14
2.2.3 Type ST	15
2.3 Rectification	15
2.3.1 Single-Phase Uncontrolled Rectifier	16
2.3.2 Three-Phase Rectifier	17

Capacitor filter, C and source inductor, L_s	18
2.4 Control Units	19
2.4.1 Automatic Reactive Power Regulator (AQR)	19
2.4.2 Automatic Power Factor Regulator (APFR)	20
2.4.3 Under-excitation Limiter (UEL)	21
2.4.4 Over-excitation Limiter (OEL)	22
2.4.5 Power System Stabilizer (PSS)	22
2.5 Basic Control Law	23
2.5.1 Proportional (P)	23
2.5.2 Integral (I)	24
2.5.3 Differential (D)	24
2.5.4 Proportional-Integral (PI)	25
2.5.5 Proportional-Differential (PD)	25
2.5.6 Proportional-Integral-Differential (PID)	26
3 Method	27
3.1 Full [®] /Simulink [®] Model	27
3.2 Synchronous Generator	28
3.3 SCR Bridge	29
3.4 Control Systems	30
3.4.1 Semiconductor Controlled Rectifiers (SCR) Control	32
3.4.2 Terminal Control	33
3.4.3 Pre-charge Control	33
3.5 Step Response SCR Bridge	34
3.6 Step Response Full Process	35
3.6.1 Additional PI-Tuning for Terminal Control	36
4 Results	38
4.1 SM Input/Output	38
4.2 Relationship between i_f and V_t	40
4.3 Bridge Output	40
4.4 SCR Control	43
4.5 SCR to Terminal Control	44
4.6 Mechanical Input Variations	45
4.6.1 PI Comparison	47
5 Discussion	48
6 Conclusions	51

Future Work 51

References **I**

Appendices **V**

 A Park transformation V

 B Simulink Model VIII

 C Ziegler-Nichols & Cohen-Coon Tuning XII

 D General XIII

Index **XV**

List of Figures

2.1	Simplified schematic of a single-phase Synchronous Machine (SM) with salient poles.	4
2.2	Simplified schematic of salient and cylindrical rotor.	5
2.3	Simplified schematic of damper winding.	6
2.4	Air-gap flux due to i_a	7
2.5	Equivalent circuit for a salient-pole rotor SM.	8
2.6	Schematic of a salient-pole SM, adapted from [1].	9
2.7	Block diagram of full excitation system, consisting of, exciter, control units and SM [10].	11
2.8	Simplified schematics of system with amplidyne. Adapted from [7].	12
2.9	Field-controlled alternator with non-controlled rectifiers, adapted from [7]. . .	13
2.10	Alternator-supplied controlled-rectifier system, adapted from [7].	14
2.11	Simplified schematics of brushless system, adapted from [7].	14
2.12	Simplified schematics of system, adapted from [7].	15
2.13	Single Phase Rectifier and its current flow.	16
2.14	Input and output voltage curves for the Single Phase Rectifier.	17
2.15	Three Phase Rectifier.	18
2.16	Three Phase Rectifier.	18
2.17	Illustration of how the capacitor smooth out the rectified voltage.	19
2.18	Single-phase bridge with source inductor L_s	19
2.19	AQR Transfer function.	20
2.20	Transfer function.	20
2.21	UEL Transfer Function Model: $Q = a + bP$ linear characteristics.	21
2.22	OEl example model.	22
2.23	ΔP Type Transfer Function Model.	23
2.24	Block diagram of transfer function of a Proportional Integral Differential (PID) control.	26
3.1	Sketch of Matlab [®] /Simulink [®] Model.	28

3.2 Thyristor block: a) Equivalen circuit b)VI characteristic. 29

3.3 Topology of SCR bridge and pre-charge system. 30

3.4 Sketch of full control system. 31

3.5 Sketch of: a) Input voltage b)Gate current 32

3.6 Sketch: Open VS Closed Loop for SCR control. 32

3.7 Sketch: Open VS Closed Loop for Terminal Control. 33

3.8 Control for the precharge system. 34

3.9 Step response for SCR bridge. 34

3.10 Dynamic response test to find the 1.order transfer function for the system. 35

3.11 Reaction Curve. 37

4.1 Constant mechanical input at 1500 Rotations per Minute (RPM). 39

4.2 Field voltage set at a reference of 90 V. 39

4.3 V_a, V_b and V_c as a result of the mechanical input and the field voltage. 39

4.4 Relationship between Field Current and Terminal Voltage. 40

4.5 Input voltage over a period of 40 ms, and $\alpha = 180^\circ$ 41

4.6 Output voltage over a period of 40 ms, and $\alpha = 180^\circ$ 41

4.7 Gate currents over a period of 40 ms, and $\alpha = 180^\circ$ 41

4.8 Input voltage over a period of 40 ms, and $\alpha = 0^\circ$ 42

4.9 Output voltage over a period of 40 ms, and $\alpha = 0^\circ$ 42

4.10 Gate currents over a period of 40 ms, and $\alpha = 0^\circ$ 42

4.11 Field voltage step up, 15 V each step. 43

4.12 Voltage step up on the terminal of the machine. 43

4.13 The current through SCR₁ while stepping up the voltage in steps of 15 V. 44

4.14 Field voltage variations, switching from SCR to terminal control. 44

4.15 Terminal voltage variations, switching from SCR to terminal control. 45

4.16 Field voltage response from decreasing the mechanical input to 1400 RPM. 45

4.17 Terminal voltage response from decreasing the mechanical input to 1400 RPM. 46

4.18 Field voltage response from increasing the mechanical input to 1500 RPM. 46

4.19 Terminal Voltage response from increasing the mechanical input to 1500 RPM. 46

4.20 Switching from SCR control to terminal control. 47

4.21 Reference change from 200 V to 230 V. 47

B.1 Full Simulink Model. VIII

B.2 Full control system. IX

B.3 Thyristor Bridge X

B.4 Synchronous Machine connected to load XI

List of Tables

2.1	Parameters for figure 2.19.	20
2.2	Parameters for figure 2.20.	21
2.3	Parameters for figure 2.21	21
2.4	Parameters for figure 2.22.	22
2.5	Parameters for figure 2.23.	23
3.1	Parameters in Matlab [®] /Simulink [®] for the SM.	28
3.2	Parameters for SCR(Adapted from datasheet.)	29
3.3	Parameters for SCR bridge.	30
3.4	Parameters for pulse generator A	31
3.5	Parameters for SCR bridge.	33
3.6	Parameters for SCR bridge.	33
3.7	Parameters for SCR bridge.	34
3.8	Dynamic response on the terminals.	35
3.9	Dynamic response on the terminals.	36
3.10	Readings for figure 3.11	36
3.11	Parameters for Ziegler-Nichols tuned regulator.	37
3.12	Parameters for Cohen-Coon tuned regulator.	37
C.1	Ziegler-Nichols tuning by using reaction curve.	XII
C.2	Cohen-Coon tuning by using reaction curve.	XII
D.1	Parameters for Terco MV1027-235.	XIII
D.2	Parameters for Thyristor/SCR.	XIV
D.3	Parameters for Terco MV1027-235.	XIV

Acronyms

AC	Alternating Current
APFR	Automatic Power Factor Regulator
AQR	Automatic Reactive Power Regulator
AVR	Automatic Voltage Regulator
D	Differential
DC	Direct Current
EMF	Electromotive Force
I	Integral
IEEE	Institute of Electrical and Electronics Engineers
OEL	Over-excitation Limiter
P	Proportional
PD	Proportional Differential
PI	Proportional Integral
PID	Proportional Integral Differential
PMSG	Permanent Magnet Synchronous Generator
PSS	Power System Stabilizer
RMS	Root Mean Square
RPM	Rotations per Minute
SCR	Semiconductor Controlled Rectifiers
SM	Synchronous Machine
Type AC	AC Excitation System
Type DC	DC Excitation System
Type ST	Static Excitation System
UEL	Under-excitation Limiter

Symbols

C	capacitor vi, 18, 30, 34
E_a	open-circuit voltage 7, 8
f	frequency 5, 17
f_N	nominal frequency 28
i_a	stator current phase-a viii, 6, 7
i_b	stator current phase-b 6
i_c	stator current phase-c 6
i_d	rotor current 6
i_f	field current 5, 6
i_q	stator current 6
K_d	differential gain 26
K_i	integral gain 24, 26
K_p	proportional gain 24, 26
L	inductor 6
L_f	field inductance 28, 30
L_{md}	Direct-axis inductance 28, 49
L_{mq}	Quadrature-axis inductance 28, 49
L_s	source inductor for the thyristor bridge vi, viii, 18, 19, 30
L_{ssm}	leakage inductance 28
n	rotations per minute 5
p	poles 5
P_N	nominal power, W 28
R_f	field resistance 28, 30
R_L	load resistor 16, 30, 34
R_s	stator resistance 28
T	period 17
V_i	input voltage for the rectifiers 16, 17
V_N	nominal voltage 28

V_o	average output voltage for the single-phase diode bridge 16, 17
ε	electromotive force 6
Φ	flux 6
λ_{ag}	total air gap flux 7
$\lambda_{aa'}$	total air gap flux linkages of phase a 7
ω	angular frequency 7, 17
α	firing angle 32, 40, 48
ε	electromotive force 6
λ	flux linkage 6

1 Introduction

A power system is a network of electrical components used to supply, consume and transfer electrical energy. The generating power plant feeds the electrical grid with power which then is consumed by the customers. When a phone charger is connected, or a big factory is starting up their machinery, everyone expects to get the power they pay for at the instant it is needed. The most common power plants convert energy from fossil fuels, nuclear fuels, and falling water, into electrical power [1].

In a power system, a lot of things can go wrong. The system is disturbed at all times by a variety of loads, and natural disasters may occur. Lightning strikes, falling trees, ice or cyclones damaging essential equipment may lead to blackout [2], [3]. Blackouts can both be expensive and dangerous, like the one in August 2003 which shut down big areas of U.S. and Canada, affecting around fifty million humans and costing several billion dollars [4], [3]. Natural disasters and events like this can never be prevented with 100% security, but protective and reliable equipment can diminish the harm.

Stable and reliable operation of power systems is a precondition for today's society. This is also a huge challenge to electrical power engineers. Deep comprehension of the power system and its components is important to maintain the system's stability. The synchronous generator is the generator that produces the majority of the electrical power [5]. In a power system, it is essential to control the voltage and ensure that the generator is always synchronized.

To keep the power system reliable, national demands and international agreements regulate both voltage and frequency in the system. In Norway, the voltage must always be within $\pm 10\%$ of the agreed voltage, and the frequency must be within $50 \pm 2\%$ Hz [6]. Europe has agreed upon a 50 Hz grid, but this is not the case all over the world; for example, in U.S., they use 60 Hz.

1.1 Literature review

The excitation system provides the field current to the rotor of the SM and by that induces the magnetic field. It provides both control and protective functions for the machine, and by this means, it provides reliability for the generator. The excitation system consists of exciter, regulators, stabilizers, limiters and protective circuits. It also protects components from exceeding their capability limits [7]. In other words, it is a composite system consisting of more than just the exciter that provides the field current. The excitation system accounts for approximately one to a few percent of the rated values for the main generator [8], so in large SMs, the excitation system may require to produce a field current of thousands of amperes, at a few hundreds of voltage [1]. The excitation system is meant to be reliable under all conditions, to be a simplicity of control, and to be easy to maintain.

In the early stage, the SM were usually implemented with a Direct Current (DC) generator as exciter source [9], and according to Institute of Electrical and Electronics Engineers (IEEE), few new ones are being built today [10]. In these kinds of systems, the regulation of excitation was usually carried out on the field winding side of the exciter, and this resulted in slow systems [5]. As technology evolved, electronic and electromagnetic regulators were introduced, and the power systems started to grow significantly and their functionalities increased. Instead of just keeping the voltage constant, they were now designed to improve the static and dynamic stability. This resulted in a more stable power system. On the other hand, the way the DC current is fed into the SM has changed little during the past century. There are some exceptions, but most of the systems still feed the field current via brushes and slip-rings. In some of the biggest SMs out there, hundreds of brushes need to be checked and maintained [11].

1.2 Objective

The objective of this master dissertation is to design an excitation system for a SM using Matlab[®]/Simulink[®]. It will take a look on the excitation systems used in power plants, which will provide substantial information surrounding the topic. A controlled rectifier will be connected to the field winding of the SM, and a sufficient control system will be implemented.

- Implementation of a SM in Matlab[®]/Simulink[®], to simulate the Terco MV1027-235 SM, stationed at Western Norway University of Applied Sciences.
- Design of AC/DC rectifier as exciter for the simulated SM.
- Design of two control systems for regulation of rectifier output, as well as controlling the three-phase terminal voltage of the SM.

1.3 Structure

The thesis will be divided into six chapters as follows:

- 2 **State of the art** This chapter takes a look into the theory behind a synchronous generator and its excitation system.
- 3 **Method** This chapter will dig further into the theory behind the chosen excitation systems and the technology used to solve the problem.
- 4 **Results** This chapter will present the simulated model.
- 5 **Discussion** This chapter will discuss the results obtained from the simulated model.
- 6 **Conclusion** This chapter will be a conclusion of the work and will present future work.

2 State of the art

This chapter will introduce some theories and existing technologies, evolving the different parts of the system designed in this thesis. The chapter starts with an introduction of the SM. Additionally, it will describe and compare different excitation systems and divide them from each other structurally and transparently. Then a brief description of the control units for the Automatic Voltage Regulator (AVR) follows. Many of the excitation systems use different kinds of rectifiers, a device that converts Alternating Current (AC) current to DC current. The theory is described in its own section. The chapter will end with an explanation about the PID controller and how different parts of the controller work.

2.1 SM Theory

An electrical machine is a device that converts electrical energy into mechanical energy or vice versa. The SM is the most common machine used as a generator to feed electrical energy into the society [12], from different energy sources such as hydro, steam, and nuclear to windmills. High reliability and cost-effectiveness are two keywords when describing this machine. Synchronous in SM addresses the fact that the rotor, along with the magnetic field created in the rotor, rotates at the same speed as the rotating magnetic field produced by the armature currents in the stator [8].

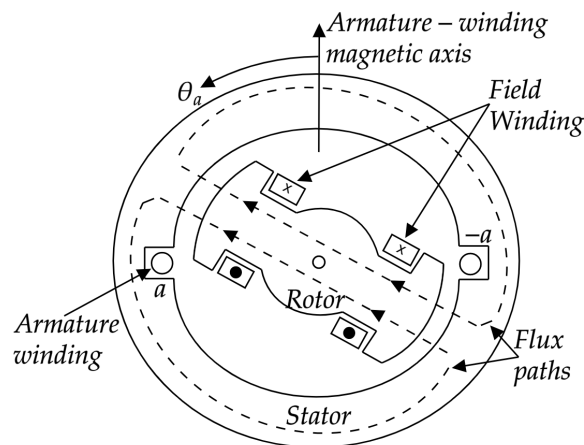


Figure 2.1: Simplified schematic of a single-phase SM with salient poles.

2.1.1 Construction

The SM consists of two main parts, the rotor, and the stator. The rotor is the rotating part of the machine, and the stator is the stationary part. The voltage is generated in the armature winding, which is found on the stator. Further on, the rotor produces the main field flux. Figure 2.1 shows a cross-section of a single-phase SM with two salient poles. The SM would normally have more than two poles. With a frequency, $f = 50\text{Hz}$, the two-pole machine would have a speed of 3000 RPM. This can be calculated by equation 2.1 [13]. The synchronous machine usually does not operate at these speeds [14].

$$n = \frac{2 \cdot 60 \cdot f}{p} \quad (2.1)$$

There are two kinds of rotors, the salient pole rotor and the round rotor, as shown in figure 2.2. In a salient pole rotor, the poles project out of the rotor core. The rotor is made out of steel lamination to reduce eddy current losses. The salient pole synchronous machine has a non-uniform air gap. Salient pole rotors are typically used at low and medium speeds, and they usually have a large number of poles. In hydroelectric power plants, the salient pole is generally used [8]. In the round rotor, there are no projected poles. The poles in this type of rotor are formed by the current flowing through the rotor excitation winding. The round rotor is typically used at high speed, and they usually use two or four poles. This makes them mechanically robust. Round rotors are often used in steam and gas power plants [8].

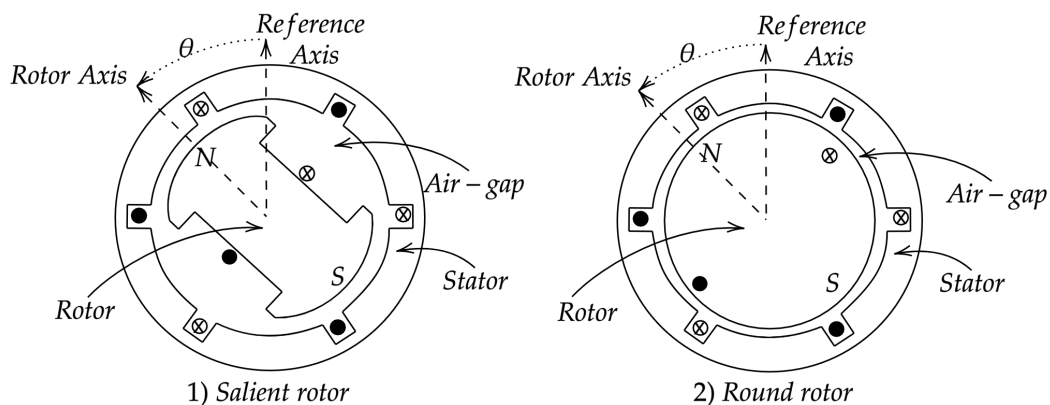


Figure 2.2: Simplified schematic of salient and cylindrical rotor.

A SM operates with two separate magnetic fields, the stator field, and the rotor field. These two rotating magnetic fields will affect each other, and an armature reaction will occur. Figure 2.1 shows where the field winding is located in the machine. This winding is getting fed by a DC current from the excitation system. This current is labeled as i_f , and the function of this current is to induce a magnetic flux in the rotor. Both the stator field and the rotor field will rotate at synchronous speed.

In a three-phase SM, there will be three armature windings, a , b and c . Figure 2.1 represents a by a coil in a single slot, and its output is represented by a' . In real life, these windings will be evenly distributed around the stator, and not only in single slots as the figure display [8]. The windings (a , b , and c) will be shifted 120° apart from each other, and they will produce a voltage that resembles a sinusoidal waveform at the terminal.

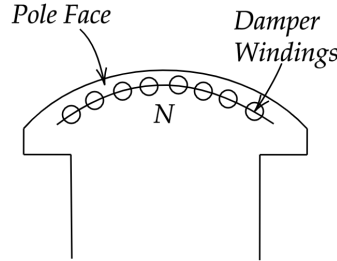


Figure 2.3: Simplified schematic of damper winding.

Damper windings are often used in SM. Their function is to damp out any oscillations that might occur. These windings are often included to help the SM to regain its synchronism after a disturbance [14]. The damper windings have a significant effect during transient conditions but in steady-state calculations the damper windings are usually ignored, hence $i_q = i_d = 0$. In figure 2.3 a simplified schematic of the windings is shown.

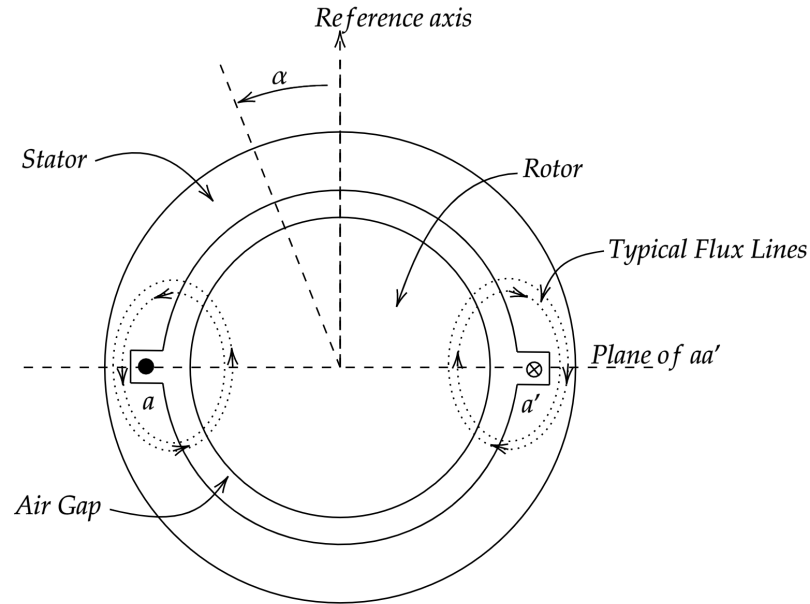
2.1.2 Voltage Generation

The generation of voltage in a SM is based on Faraday's law. This law states that the Electromotive Force (EMF) or the induced voltage is given by the rate of change of the magnetic flux. The ε is given by equation 2.3. The voltage induced in a closed-loop inductor is proportional to the total flux change through the inductor loop. Since this is true, the flux Φ will be equal to the total flux linkages λ . The flux linkages are given by equation 2.3, where the inductor L is the proportionally constant between the current and the flux linkages.

$$\varepsilon(t) = -\frac{d\Phi(t)}{dt} = -\frac{d\lambda(t)}{dt} \quad (2.2)$$

$$\Phi(t) = Li(t) \quad (2.3)$$

Neglecting the leakage flux, the flux which does not cross the air gap, and considering only the air-gap flux, the air-gap flux is only dependent on the field current i_f and the stator currents i_a , i_b and i_c [1]. To find the total air gap flux, an assumption that the magnetic circuit is linear is made. This makes it possible to use superposition by considering the flux linkages due to i_f alone ($i_a = i_b = i_c = 0$), and then to i_a , i_b and i_c alone ($i_f = 0$). These two flux

Figure 2.4: Air-gap flux due to i_a .

linkage components will give two voltage components, the open-circuit voltage and the armature reaction voltage. These voltages will, in sum, give us the air-gap voltage due to the total air-gap flux [1]. The open-circuit voltage is the voltage in the SM while no load is connected and no current flowing through the stator coils. The armature voltage is the voltage that is induced due to the current that flows in the stator coils. Three fluxes are defined [1]. λ_{ag} is defined as the total air gap flux linkages of coil aa' , $\lambda_{aa'}$ is defined as the total air gap flux linkages of phase a, and λ_{ar} is defined as the armature reaction flux linkages. The air gap flux and the air gap voltage are written in phasor form in equation 2.4 and equation 2.6. Equation 2.5 gives the armature reaction flux linkages in phasor form. These equations are valid for a round rotor SM since the air gap is uniform(see figure 2.4).

$$\lambda_{ag} = \lambda_{aa'} + \lambda_{ar} \quad (2.4)$$

$$\lambda_{ar} = L_s I_a \quad (2.5)$$

$$V_{ag} = E_a - j\omega_0 L_{s1} I_a \quad (2.6)$$

where E_a is the open circuit voltage, V_{ag} is the generated voltage, and L_{s1} is a fictitious inductance. Accounting for the resistance, r and leakage reactance, X_s , in the windings, the

terminal voltage, V_a , for a round rotor machine is given:

$$V_a = E_a - rI_a - jX_s I_a \quad (2.7)$$

In a salient pole SM where the air gap is not uniform, see figure 2.2, another set of equations is needed. This means that the length of the air gap will change with the rotation of the rotor, which makes the flux linkage vary. To handle this problem, the armature reaction is decomposed along two axes, one along the direct axis of the rotor and another along the quadrature axis, which is orthogonal to the direct axis. The direct axis components are marked with subscripts letter d , and the quadrature axis components are marked with the subscript letter q . This is called a park-transformation, which is a way of representing a set of three sinusoidally-varying phase currents and voltages (a , b and c), using only two values (d and q) [15] [16]. The full park transformation can be found in appendix A. The corresponding flux linkages of coil aa' in phasor form is given by equation 2.8.

$$\Lambda_{ar} = \Lambda_{ad} + \Lambda_{aq} \quad (2.8)$$

$$\Lambda_{ad} = L_{d1} I_{ad} \quad (2.9)$$

where L_{d1} is the inductance and, I_{ad} is the current, on fictitious winding d .

$$\Lambda_{aq} = L_{q1} I_{aq} \quad (2.10)$$

where L_{q1} is the inductance and, I_{aq} is the current, on fictitious winding q .

The terminal phase voltage of phase a for a salient-pole SM is given by equation 2.11 and the equivalent circuit are shown in figure 2.5.

$$V_a = E_a - rI_a - jX_d I_{ad} - jX_q I_{aq} \quad (2.11)$$

where X_d and X_q is the reactance on the direct and quadrature axis, respectively.

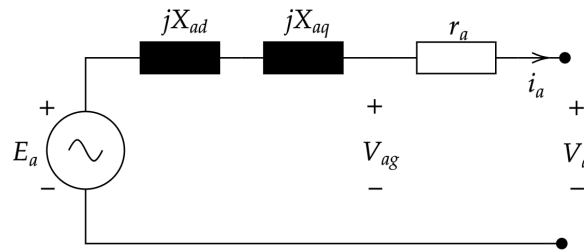


Figure 2.5: Equivalent circuit for a salient-pole rotor SM.

2.1.3 Park Transformation

The park transformation represents a set of 3 sinusoidally-varying phase currents and voltages using only two values. This method greatly simplifies the modeling of the synchronous generators. In 1929 and 1933, R.H. Park published two articles considering the Park transformation. These articles proposed a method that converted the stator variables into equivalent rotor variables [15], [16]. This was a whole new approach to electric machine analysis.

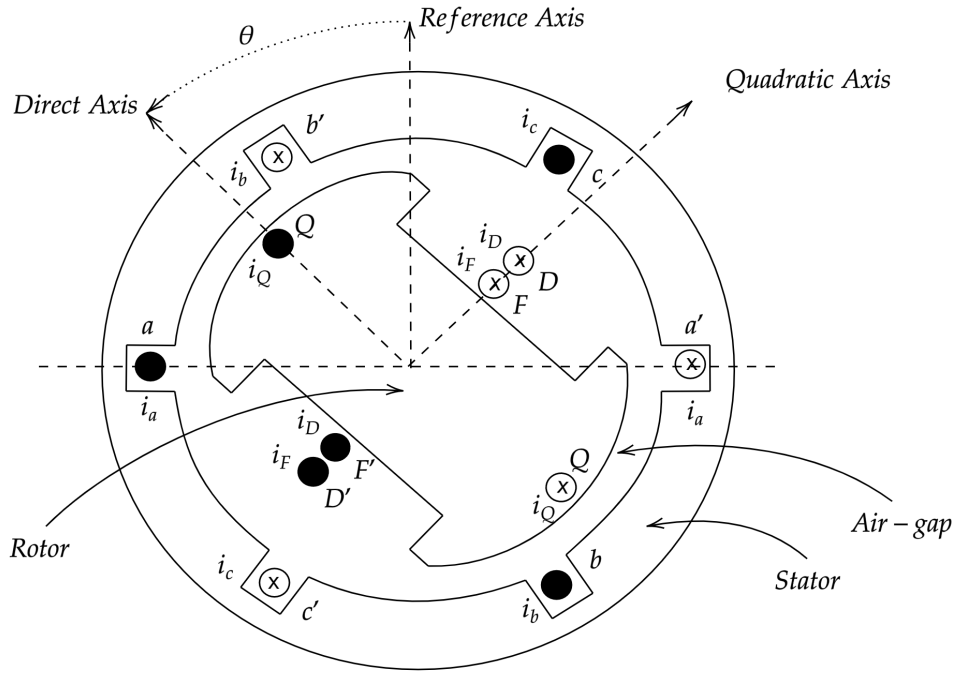


Figure 2.6: Schematic of a salient-pole SM, adapted from [1].

Figure 2.6 shows an three-phase synchronous machine with two fictitious windings, the direct and quadrature axes. The voltages on the terminal and for the direct and quadrature axis are shown in equation 2.13.

$$\mathbf{v} = -\mathbf{R}\mathbf{i} - \frac{d\boldsymbol{\lambda}}{dt} \quad (2.12)$$

Where \mathbf{v} is the voltage vector consisting of the terminal voltages (v_a, v_b, v_c), the field voltage (v_F) and the damper voltages (v_D and v_Q). \mathbf{i} is the corresponding current vector, \mathbf{R} is a 4×4 matrix, and $\boldsymbol{\lambda}$ is the flux linkages. The equation can be written as:

$$\begin{bmatrix} v_a \\ v_b \\ v_c \\ -V_F \\ -V_D \\ -V_Q \end{bmatrix} = \begin{bmatrix} r & & & & & \\ & r & & & & \\ & & r & & & \\ & & & r_F & & \\ & & & & r_D & \\ & & & & & r_Q \end{bmatrix} \begin{bmatrix} i_a \\ i_b \\ i_c \\ i_F \\ i_D \\ i_Q \end{bmatrix} - \frac{d}{dt} \begin{bmatrix} \lambda_{aa'} \\ \lambda_{bb'} \\ \lambda_{cc'} \\ \lambda_{FF} \\ \lambda_{DD} \\ \lambda_{QQ} \end{bmatrix} \quad (2.13)$$

Where $\lambda_{aa'}$, $\lambda_{bb'}$, $\lambda_{cc'}$, λ_{FF} , λ_{DD} , λ_{QQ} is the flux linkages. Where the variables with lower case letters is the stator variable, and the variable with upper case letters is the rotor variable. By using equation 2.3, equation 2.14 represents the flux linkages. The majority of the inductances shown in this equation are dependent on the placement of the rotor, and thus they will change with time. All of the equations for these are shown in appendix A.

$$\begin{bmatrix} \lambda_{aa'} \\ \lambda_{bb'} \\ \lambda_{cc'} \\ \lambda_{FF} \\ \lambda_{DD} \\ \lambda_{QQ} \end{bmatrix} = \begin{bmatrix} L_{aa} & L_{ab} & L_{ac} & L_{aF} & L_{aD} & L_{aQ} \\ L_{ba} & L_{bb} & L_{bc} & L_{bF} & L_{bD} & L_{bQ} \\ L_{ca} & L_{cb} & L_{cc} & L_{cF} & L_{cD} & L_{cQ} \\ L_{Fa} & L_{Fb} & L_{Fc} & L_{FF} & L_{FD} & L_{FQ} \\ L_{Da} & L_{Db} & L_{Dc} & L_{DF} & L_{DD} & L_{DQ} \\ L_{Qa} & L_{Qb} & L_{Qc} & L_{QF} & L_{QD} & L_{QQ} \end{bmatrix} \begin{bmatrix} i_a \\ i_b \\ i_c \\ i_F \\ i_D \\ i_Q \end{bmatrix} \quad (2.14)$$

Where i_a , i_b , i_c , i_F , i_D and i_Q is the current flowing in each winding. Applying the park transformation on equation 2.14 (the transform can be found in appendix A), the time-dependent variables are eliminated and the equation can be rewritten to equation 2.15. The matrix now consists of only constant variables.

$$\begin{bmatrix} \lambda_0 \\ \lambda_d \\ \lambda_q \\ \lambda_F \\ \lambda_D \\ \lambda_Q \end{bmatrix} = \begin{bmatrix} L_0 & 0 & 0 & 0 & 0 & 0 \\ 0 & L_d & 0 & kM_F & kM_D & 0 \\ 0 & 0 & L_q & 0 & 0 & kM_Q \\ 0 & kM_F & 0 & L_D & L_{FD} & 0 \\ 0 & kM_D & 0 & M_R & L_F & 0 \\ 0 & 0 & kM_Q & 0 & 0 & L_Q \end{bmatrix} \begin{bmatrix} i_a \\ i_b \\ i_c \\ i_F \\ i_D \\ i_Q \end{bmatrix} \quad (2.15)$$

Where λ_0 , λ_d , λ_q , λ_F , λ_D , λ_Q is the flux linkage of each winding. L_0 , L_d , L_q , L_D , L_F , L_Q is the self inductance of each winding. M_F , M_D , M_Q , M_R represents the mutual inductance between the windings [17]. Windings are shown in figure 2.6.

2.2 Excitation System

The SM is dependent on a magnetic field to be able to generate power. The excitation system does this, by feeding DC current into the field winding of the machine. The system works as a feedback control system and is usually operated with various kinds of PID controllers. As technology evolves, it has gotten more and more functions in the power system. Today the excitation system controls the voltage, the field current, the power factor, and the reactive power. It also functions as a protection of the SM and for the excitation system itself [18] [5]. Hence the excitation system carries out both control and protective functions.

The excitation system is used to describe an entire system usually consisting of an AVR, exciter, measuring elements, power system stabilizer, excitation limiters, and protection units. See figure 2.7. The exciter is the source of the excitation current, and this source varies from system to system. The source can be realized by a DC generator, which feeds the main SM directly, or it can be an AC generator which produces a three-phase current which is then rectified by the use of diodes, thyristor or transistor bridge [19]. There are also self-excited systems that get their excitation current from the main generator itself, based on controlled rectifiers [9].

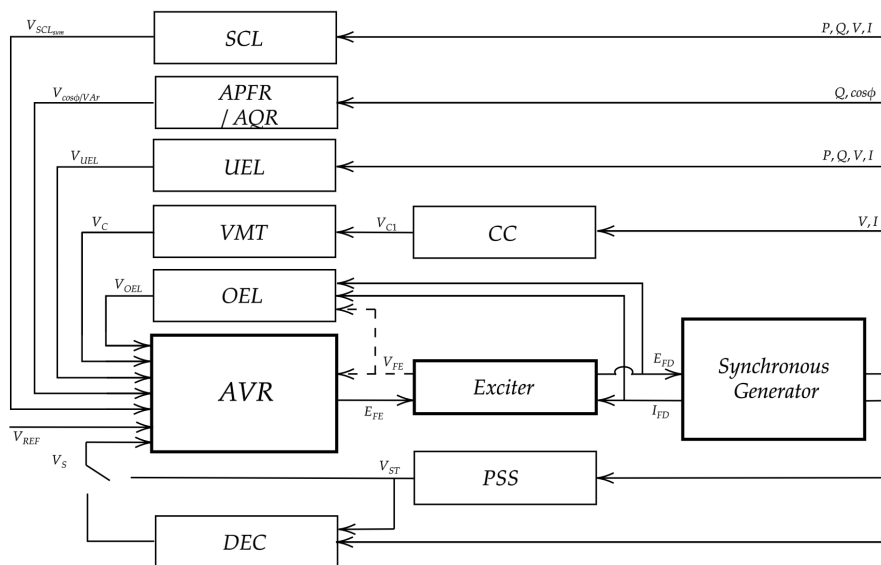


Figure 2.7: Block diagram of full excitation system, consisting of, exciter, control units and SM [10].

This thesis will classify the systems based on the excitation power source, in the same manner as IEEE Std 421.5TM IEEE:

- **DC Excitation System (Type DC)** - DC generator as the source of excitation power.
- **AC Excitation System (Type AC)** - AC generator as the source of excitation power.

- **Static Excitation System (Type ST)** - Excitation power is supplied via transformer and rectifiers.

2.2.1 Type DC

This kind of system uses a DC generator as the source of excitation power. The output of the exciter is fed into the main SM through slip rings [20], [7]. In large systems where the main generator produces a lot of power, a pilot exciter might be needed for the exciter. In these cases, the system will have one main exciter, which provides the excitation current to the main SM and the pilot exciter, a self-excited machine that provides field current to the main exciter. In some cases, the exciter is self-excited. Many systems in service today still use this excitation system, but few new ones are being built [10]. The area for this kind of system was between the 1920s and 1960s, and by the mid-60s they were more and more replaced by the Type AC systems [7].

A simplified block-diagram of a Type DC system is represented in figure 2.8. It shows the main exciter as a DC generator which supplies the DC current into the field winding of the controlled SM. In this example, an amplidyne is feeding the DC generator with field current. An amplidyne is the most common form of the metadyne, which is an electrical machine with two pairs of brushes. The device got high amplification and fast speed of response [21]. The amplidyne provides the exciter field, in a so called "buck-boost" scheme, and the rest of the required field is made by self-excitation [7]. If the amplidyne in figure 2.8 is out of service, the system can adjust the exciter field manually through the rheostat.

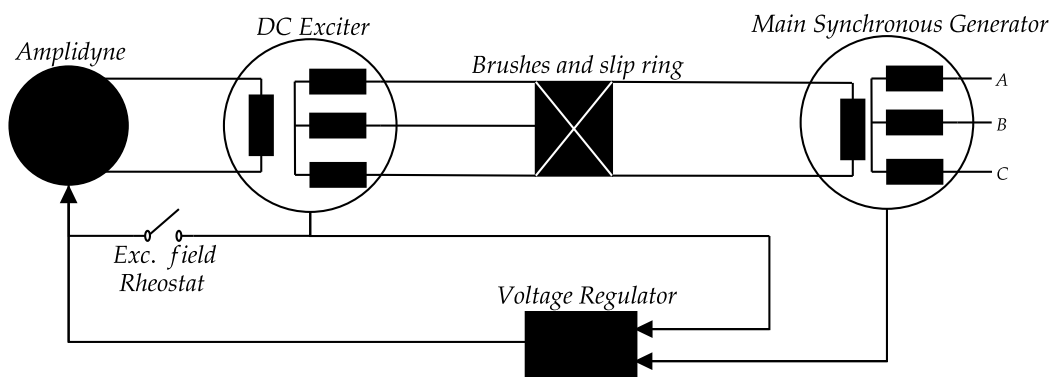


Figure 2.8: Simplified schematics of system with amplidyne. Adapted from [7].

2.2.2 Type AC

In this system the source of excitation power comes from an AC machine with rectifiers connected to the output of the exciter. The rectifiers can either be stationary or rotating. The rectifiers convert the AC to DC and they can be both controlled or non-controlled, depend-

ing on the system. This system can be built in various forms, depending on rectifiers used, source of excitation for the exciter, and the applied methodology of control [7]. It is common to divide these system into two groups; stationary rectifiers and rotating rectifiers.

Stationary rectifiers

The systems with stationary rectifiers are in need of sliprings and brushes for the delivery of excitation current to the generator. If the system is to use non-controlled rectifiers (e.g. diodes), a regulator is used to control the field of the AC-exciter [7]. An example of a system like this is represented in figure 2.9. In this example, the exciter is self-excited by the means of controlled-rectifiers (e.g. thyristors), and the three-phase output of the exciter is rectified by the non-controlled bridge. Later on the DC is then fed into the field winding of the controlled SM through brushes and slip rings.

Another example of a stationary Type AC system is shown in figure 2.10. In this system the exciter is no longer self-excited, but the exciter is in need of an pilot-exciter. The pilot-exciter is self-excited through controlled-rectifiers and controlled by the regulator. As shown in the figure, the AC exciter is feeding its power to another set of controlled-rectifier, which then convert the three-phase AC into DC. The most common controlled-rectifiers are based on thyristors, because of their high power handling capabilities [22]. The regulators in figure 2.10 control the DC directly through the thyristor-bridge.

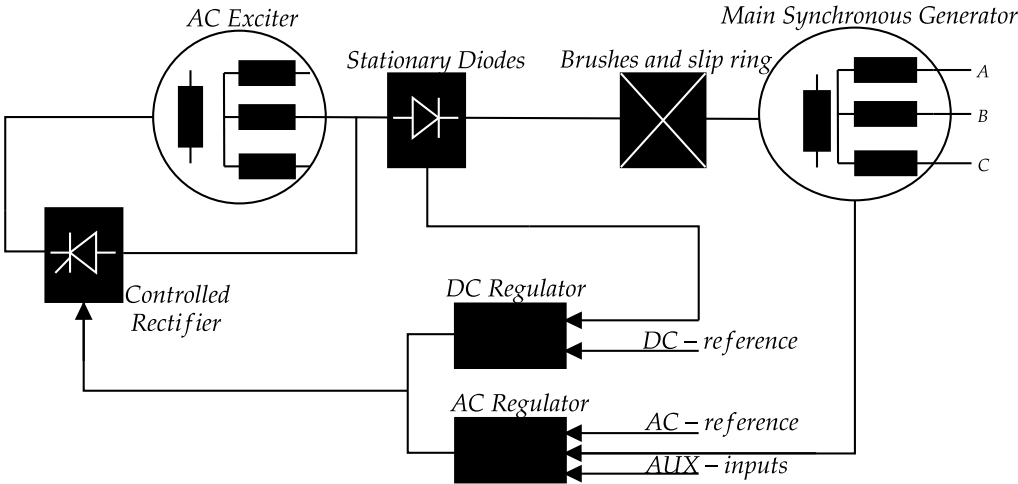


Figure 2.9: Field-controlled alternator with non-controlled rectifiers, adapted from [7].

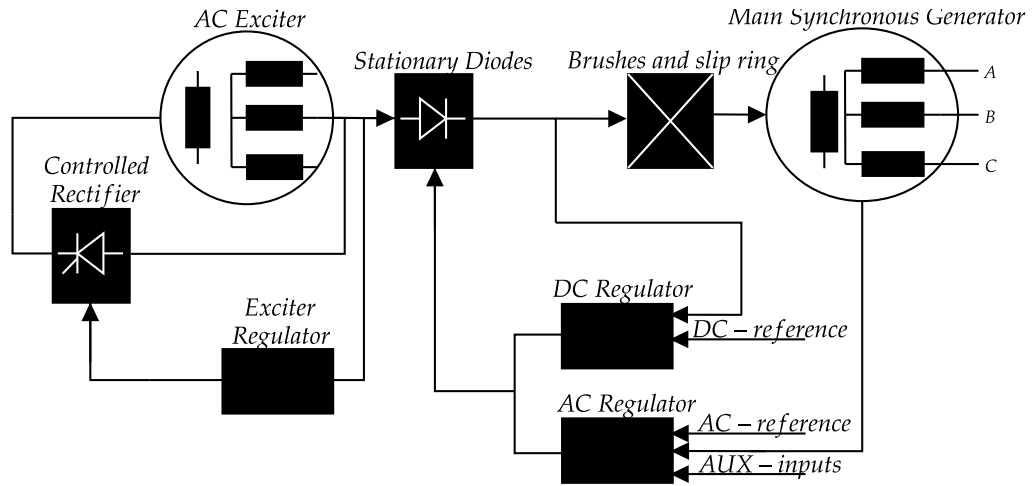


Figure 2.10: Alternator-supplied controlled-rectifier system, adapted from [7].

Rotating rectifiers

In the manner of rotating rectifiers, there are no need of brushes [7], [23]. This system is most often referred to as a brushless excitation system. These brushless systems are often used in smaller hydro-power plants, maritime facilities, and in industrial systems [23]. They still use an AC generator as source of excitation, and this power is then rectified to a DC current. The DC current is then fed directly into the field winding of the controlled SM. The name comes from the fact that the rectifier along with the armature of the exciter, rotates, see figure 2.11. This system requires a pilot-exciter, which feeds the AC exciter, in figure 2.11 a Permanent Magnet Synchronous Generator (PMSG) is uses as a pilot exciter.

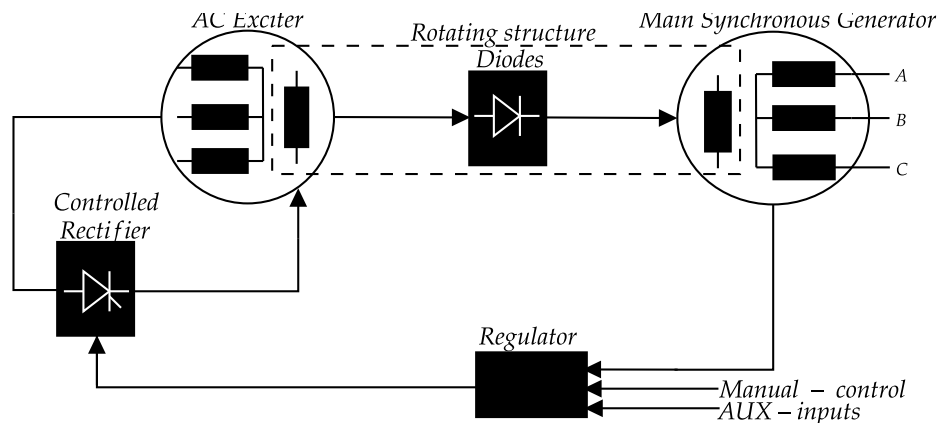


Figure 2.11: Simplified schematics of brushless system, adapted from [7].

This system was originally developed to avoid the use of brushes and slirings. Nevertheless, it seems like the brushless Type AC performs equally well as the Type AC systems that uses brushes [7].

2.2.3 Type ST

The static excitation system is one of the most typical excitation system in big hydro-power plants [23]. The name of this system comes from the fact that all the components are static or stationary. Common for these systems is that the excitation power is fed either from the main terminals of the controlled SM or from the station auxiliary bus. This system can in other words be described as a self-excited system. This power is fed through a transformer which then feeds either a controlled, or a non-controlled rectifier which regulates the voltage. Since this is a self-excited system, the system needs an additional source of power to get it started. The SM cannot produce any voltage without any field current. This process of build-up for the generator field-flux is termed field flashing [24], [7].

Figure 2.12 shows an example of a Type ST system. The power for the exciter is taken from either the terminals of the main SM itself, or the station auxiliary bus. An excitation transformer is connected to the output of the terminal and steps down the voltage and feeds the AC voltage into a controlled-rectifier. This system is also known as a bus-fed or transformer-fed excitation system. The controlled-rectifier is then transforming the AC current to DC current and feeds the field winding of the main SM via brushes. This system is both inexpensive and it is easily maintainable[7].

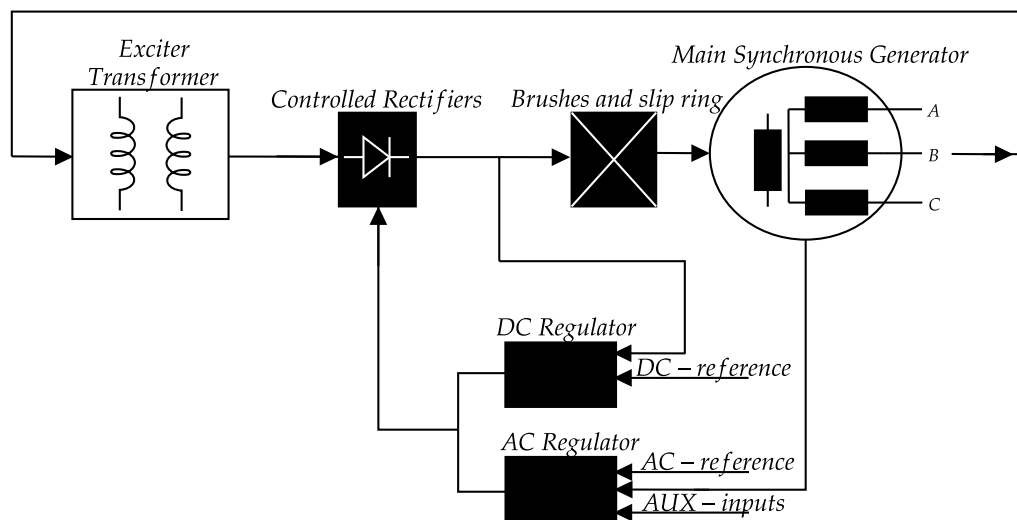


Figure 2.12: Simplified schematics of system, adapted from [7].

2.3 Rectification

Rectifiers are widely used in practical applications, such as computers and battery chargers. [25]. Both Type AC and Type ST systems use rectifiers in their excitation systems. In the excitation systems out there, the three-phase bridge is the most common to use and has cur-

rently become the only selected one [5]. The function of a rectifier is to convert AC current to DC current. If the operation is reversed the device is called an inverter. Rectifiers are made possible by the unique features of semiconducting devices. In simple terms, a semiconducting device can pass the current in one direction and block it or slow it down in the opposite direction. They can also be controlled or uncontrolled, depending on the chosen semiconductor. In this subsection both the single- and three-phase rectifier, based on diodes, will be discussed.

2.3.1 Single-Phase Uncontrolled Rectifier

The circuit in figure 2.13 represents an uncontrolled single-phase full wave rectifier. This is an uncontrolled device, since it uses the simplest form of semiconductors, four diodes. The diode cannot be controlled, and in simple terms it can conduct in one direction (forward biased) and block in the opposite direction (reverse biased).

The uncontrolled single-phase full-wave rectifier rectifies the full sinusoidal AC current and converts it into a DC current. The bridge configuration makes it possible to convert both the positive and negative half cycle of the sinusoidal wave. In the circuit two of the four diodes will always be forward bias, and two of them will always be reverse biased. When a diode is forward bias, it conducts current, and when its reverse biased it blocks the current.

Figure 2.13 shows how the current flow in a single-phase rectifier. The left part of the figure represents the positive half cycle of the sinusoidal AC. In this state D_1 and D_4 are forward biased, and D_2 and D_3 are reversed biased. The current will then flow from the source, through D_1 , R_L , D_4 and back to the source. The right part represents the negative half cycle. In this state, D_1 and D_4 turn reverse biased and block the current, while D_2 and D_3 switching to forward bias. Here the current will flow from the source, through D_3 , R_L , D_2 and back to the source [26].

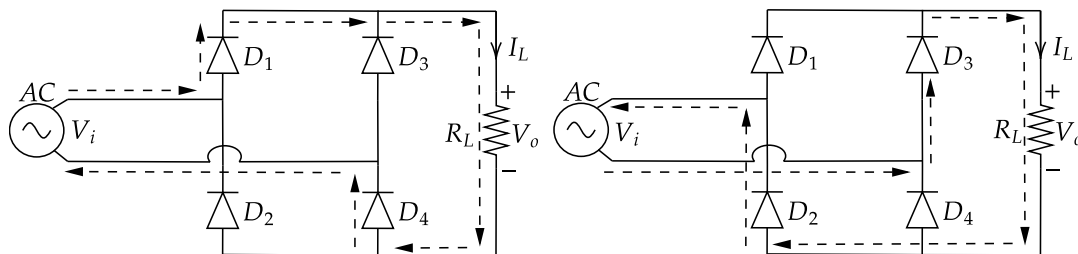


Figure 2.13: Single Phase Rectifier and its current flow.

Figure 2.14 represents the waveform of both the input and the output voltage. The sinusoidal black curve represents the input voltage, V_i , and the below curve represents the output, V_o . As shown in this figure, the output voltage will not be a pure straight line, as we might think

of a DC. The voltage from the rectifier will have some ripples as a result of the alternating supply. These ripples can be modified by the use of different kind of snubber circuits.

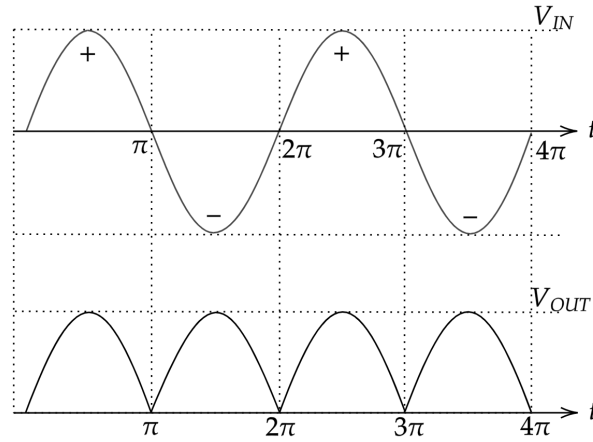


Figure 2.14: Input and output voltage curves for the Single Phase Rectifier.

The bridge above represents an ideal circuit. The average voltage of an ideal single-phase rectifier is given by equation by:

$$V_o = \frac{1}{T/2} \int_0^{T/2} \sqrt{2}V_i \sin \omega t \, dt = \frac{1}{\omega T/2} (\sqrt{2}V_i \cos \omega t) = \frac{2}{\pi} \sqrt{2}V_i \quad (2.16)$$

$$V_o = \frac{2}{\pi} \sqrt{2}V_i = 0.9V_i \quad (2.17)$$

Where V_i is the AC input measured in rms, $\omega = 2\pi f$ and $\omega T/2 = \pi$ [22] [26].

2.3.2 Three-Phase Rectifier

The three phase rectifier is based on the same principle as the single phase one. This rectifier is widely used in practice [27]. These voltages can be seen on like three phases that are 120 electrical degrees ahead of each other. The advantages here is that the output voltage will have less ripple in comparison to a single-phase input, see figure 2.15.

The rectifier which will be described in this section is also an uncontrolled-rectifier made out of diodes. In the same manner as the single-phasen it can be made out of transistors and thyristors, and it will then require some sort of control to function. This circuit is widely used in both the Type AC and Type ST excitation systems [5].

Figure 2.15 shows the full bridge consisting of six diodes, which must be considered to be an idealized circuit. To get to the average output DC only one of the segments in figure 2.16 is considered, that means a period of $360^\circ/6 = 60^\circ$ is set to be the interval. To get the average voltage for an idealized circuit represented in equation 2.18 to 2.20 [22]. V_{LL} is the rms value

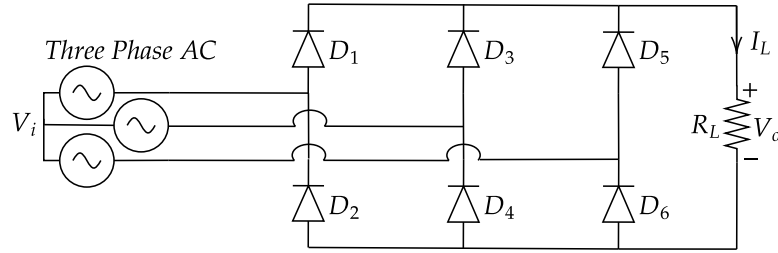


Figure 2.15: Three Phase Rectifier.

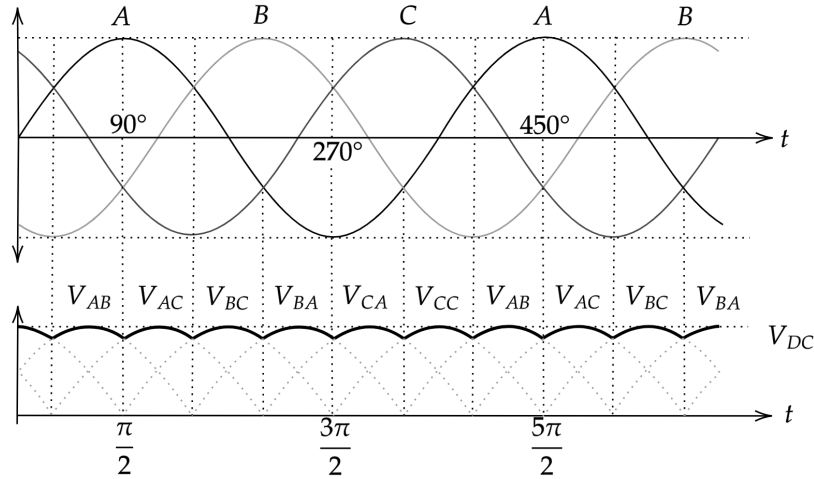


Figure 2.16: Three Phase Rectifier.

on the line-to-line voltage and A is the area under the chosen segment.

$$v_o = v_{ab} = \sqrt{2}V_{LL} \cos \omega t \quad -\frac{1}{6}\pi < \omega t < \frac{1}{6}\pi \quad (2.18)$$

$$A = \int_{-\pi/6}^{\pi/6} \sqrt{2}V_{LL} \cos \omega t \, d(\omega t) = \sqrt{2}V_{LL} \quad (2.19)$$

$$V_o = \frac{1}{\pi/3} \int_{-\pi/6}^{\pi/6} \sqrt{2}V_{LL} \cos \omega t \, d(\omega t) = \frac{3}{\pi} \sqrt{2}V_{LL} = 1.35V_{LL} \quad (2.20)$$

Capacitor filter, C and source inductor, L_s

In practical rectifiers a capacitor filter is often used for smoothing the output voltage. The rectified voltage will energize the capacitor as long as the input voltage is superior to the capacitor voltage. The capacitor will charge until it reaches the peak value for the input voltage, and discharge when the AC voltage falls under the capacitor voltage. This will result in a more stable output for the system.

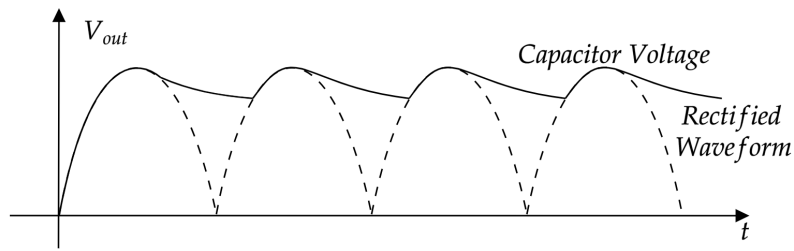


Figure 2.17: Illustration of how the capacitor smooth out the rectified voltage.

Figure 2.17 shows how the capacitor filter changes the output of the bridge. The stippled lines represents the rectified waveform without the filter, and the black line represents the capacitor voltage. When the voltage is rising the capacitor is charged up and when the voltage decreases the capacitor is discharging. By increasing the capacitor value the output voltage will be more and more similar to a DC current.

To get a understanding of why a source inductor is needed a simplified circuit is shown in figure 2.18.

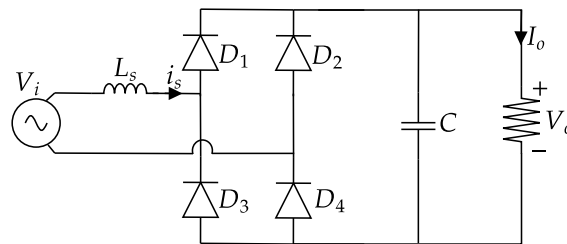


Figure 2.18: Single-phase bridge with source inductor L_s .

When a diode bridge, described in section 2.3, is running without any source inductance, an assumption has been stated that the currents transfer from one diode to another immediately. This is not true for practical rectifiers with a AC source that got some inductance L_s to it. The change of current must now take some time to happen. This is called commutation or overlap process, and this forces all the diodes in the circuit to conduct at the same time. When all the diodes are conducting the output voltage will be zero and all of the input voltage will apply across L_s .

2.4 Control Units

2.4.1 AQR

As the name suggest, the AQR is applied to regulate the reactive power of the controlled unit. The use of both AQR and APFR, has its origin in industrial applications of synchronous

motors and generators. Large generators connected to the bulk power systems, the use of both AQR and APFR are usually forbidden according to constrains [10]. The expression of the AQR is given in equation 2.21 [5]. a, b and c are coefficients determined on the basis of the operational requirements. P and Q is the active and reactive power, respectively.

$$Q = a + bP + cP^2 \tag{2.21}$$

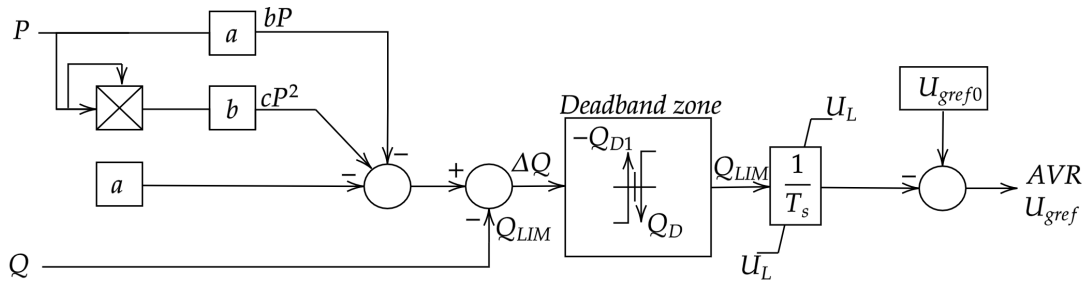


Figure 2.19: AQR Transfer function.

Table 2.1: Parameters for figure 2.19.

Symbol	Meaning	Symbol	Meaning
$T(s)$	Rate of changes for the voltage setting device	$Q_{LIM}(p.u.)$	AQR output
Q_D	Deadband zone	$\pm U_L(p.u.)$	Integral limit

2.4.2 APFR

The APFR is a system which is used to control the power factor of the synchronous generator. This could be to keep the power factor at a set value or within a set range. The transfer function model is shown in figure 2.20, the output of the block is going to the AVR.

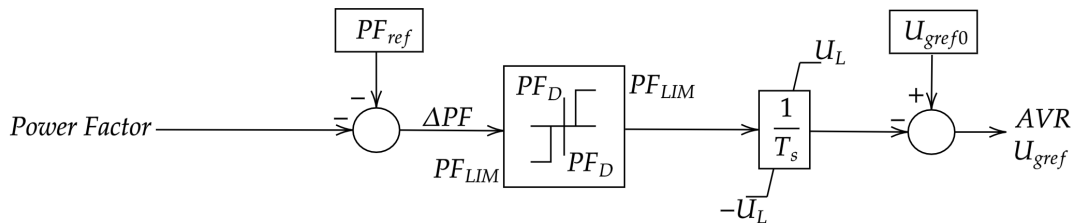


Figure 2.20: Transfer function.

Table 2.2: Parameters for figure 2.20.

Symbol	Meaning	Symbol	Meaning
$T(s)$	Rate of change for the voltage setting device	$PF_{LIM}(p.u.)$	APFR output
PF_D	Deadband zone	$\pm U_L(p.u.)$	Integral limit

2.4.3 UEL

The UEL is used to protect the generator from losing synchronism and to prevent operation that could lead to overheating in the stator region of the synchronous machine [10]. There are different kind of UELs, where some uses a combination of voltage and current, and some uses a combination of active and reactive power. -The linear expression of the UEL is expressed in equation 2.22 . In this equation, a and b are parameters determined by the limit characteristic [5]. For the linear limit characteristics, the transfer function model is shown in figure 2.21. The output of this block is sent to the AVR.

$$Q = a + bP \quad (2.22)$$

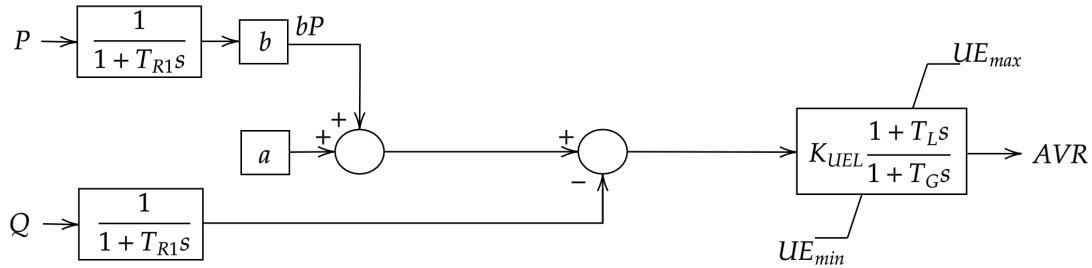
Figure 2.21: UEL Transfer Function Model: $Q = a + bP$ linear characteristics.

Table 2.3: Parameters for figure 2.21

Symbol	Meaning	Symbol	Meaning
$T_{R1}(s)$	Time constant for the P transducer	K_{UEL}	UEL gain
$T_{R2}(s)$	Time constant for the Q transducer	$T_L(s)$	Time constant for the leading phase compensation
UE_{max}	Upper output limit	$T_G(s)$	Time constant for the lagging phase compensation
UE_{min}	Lower output limit		

There are different kinds of UELs but these will not be discussed here.

2.4.4 OEL

OELs are often referred to as maximum excitation limiters and field current limiters [10]. The OEL is used as protection to prevent the generator rotor excitation winding from overheating [5]. The detection signal varies with different excitation modes. Generator excitation current and voltage, and the exciter excitation current are included in these excitation modes. An example of an OEL model is shown in figure 2.22. According to IEEE Std421.5, OEL modeling should not be required in most system studies [10].

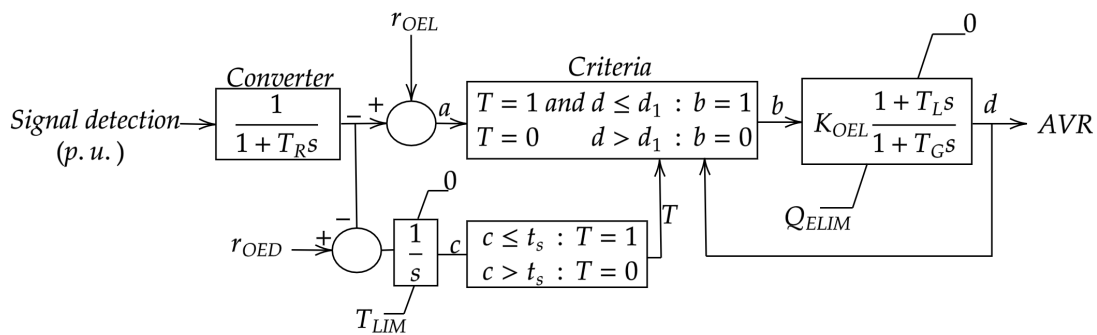


Figure 2.22: Oel example model.

Table 2.4: Parameters for figure 2.22.

Symbol	Meaning	Symbol	Meaning
$T_R(s)$	Time constant for the transducer	$a_1(p.u.)$	Return difference value for operation reset
$r_{OEL}(p.u.)$	Limited target value	$T_{LIM}(p.u.)$	Integral limit value
$r_{OED}(p.u.)$	Initial value for OEL operation	$Q_{ELIM}(p.u.)$	Max.limit value
t_s	Timing value for OEL operation	$T_G(s)$	Time constant for the lagging phase compensation
K_{OEL}	OEL gain	T_{OEL}	Integral time constant
$T_L(s)$	Time constant for the leading phase compensation	d_1	Min. detection value for guaranteed operation

2.4.5 PSS

The PSS are used to enhance damping of power system oscillations. This is done through excitation control. The most common used inputs are shaft speed, terminal frequency and

power [10]. PSS can then be divided into three types. ΔP -type which uses the power as input, $\Delta\omega$ -type which uses the shaft speed and Δf -type which uses the frequency as input. The transfer function model of an example of a ΔP -type is shown in figure 2.23 [5].

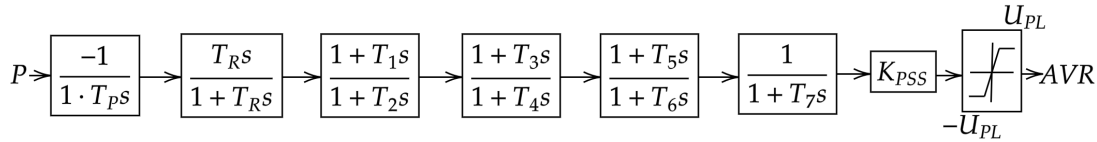


Figure 2.23: ΔP Type Transfer Function Model.

Table 2.5: Parameters for figure 2.23.

Symbol	Meaning	Symbol	Meaning
$T_P(s)$	Time constant for the active power P detector	$T_3(s)$	Time constant for the leading phase compensation
$T_R(s)$	Time constant for the isolation filter	$T_4(s)$	Time constant for the lagging phase compensation
$T_1(s)$	Time constant for the leading phase compensation	K_{PSS}	PSS gain
$T_2(s)$	Time constant for the lagging phase compensation	$U_{PL}(p.u.)$	PSS output limit

2.5 Basic Control Law

The basic control law of the excitation controller has three factors controlling the system [5]. The proportional (P), the integral (I), the derivative (D), and the combination of these. Combination of these would result in the Proportional Integral (PI)-, Proportional Differential (PD)- and the PID - controllers. PID controller comes with several advantages: ease of use, stable and reliable and simple structure. These controllers are used in all kinds of industrial control systems [28]. The PID controller is the most common control used in excitation systems [29]. Each letter in the name got their own function, and if one function is not needed in the PID controller it can simply be set to zero.

2.5.1 P

A proportional controller is based on a response in proportion to the difference between the desired value and the current value of the variable. This kind of control system is used in many industrial settings and it is also used in some smart devices. Proportional control

is a feedback control system, where correction is applied to the controlled variable which is proportional to the difference between the set value. The proportional term is given by equation 2.23. The transfer function of the proportional controller is given by equation 2.24.

$$u(t) = K_p e(t) \quad (2.23)$$

$$G_c(s) = \frac{U(s)}{E(s)} = K_p \quad (2.24)$$

Where $U(s)$ is the Laplace transform of the output, $E(s)$ is the laplace transform of the input and K_p is the proportional gain of the controller [5]. By increasing K_p , the sensitivity of the system increases, and by that the system will respond faster compared to a lower K_p . This does not mean that the higher K_p the better, because if it gets too high values the system will become unstable [28].

2.5.2 I

The integral term I, is proportional to the magnitude and the duration of the error signal. It is the sum of the instantaneous error over time and gives the offset that should have been corrected previously. The error is then multiplied by the integral gain K_i and then added to the output of the system. The function of adding the integral term is to accelerate the movement of the process towards set-point and the term eliminates residual steady-state error that occurs with a pure proportional controller. The integral controller can however cause the present value to overshoot the set-point value. Too high integral gain will also here lead to an unstable system [28]. The integral term is shown in equation 2.25. The transfer function is expressed in equation 2.26 [5]. The disadvantages of the pure integral controller is that it cannot keep the output u and the input e synchronized and quick to respond. The output changes will always lag behind the deviation changes [5].

$$u(t) = K_I \int_0^t e(\tau) d\tau \quad (2.25)$$

$$G_c(s) = \frac{U(s)}{E(s)} = \frac{K_i}{s} \quad (2.26)$$

2.5.3 D

Some controlled systems require a more advanced regulation. These objects are usually adopted according to the variation trend of the controlled variable to avoid generating much

greater deviation during the regulation [5]. This leads to the differential control law which is expressed by equation 2.27. The controller output $u(t)$ and the rate of change in the input deviation $de(t)/dt$ are in proportion, and the proportional factor T_D is the differential time constant. The differential controller cannot be used as a standalone control system, it is always combined with the proportional controller as a PD- or a PID-controller. This controller is able to predict the systems behaviour and thus improve settling time and the stability of the system. The transfer function is expressed in equation 2.28:

$$u(t) = T_D \frac{d}{dt} e(t) \quad (2.27)$$

$$G_c(s) = T_D s \quad (2.28)$$

2.5.4 Proportional-Integral (PI)

The PI-controller is a combination of the proportional and the integral controller. This controller combines the quick response of the proportional controller, and the elimination of steady-state error by the integral controller. Equation 2.29 expresses the control law of the PI-controller, while equation 2.30 expresses the transfer function. The proportional term is represented by $K_P e(t)$ and the integral term is represented by $\frac{K_P}{T_I} \int_0^t e(t) dt$. T_I is the integration time constant [5].

$$u(t) = K_P \left[e(t) + \frac{1}{T_I} \int_0^t e(t) dt \right] \quad (2.29)$$

$$G_c(s) = \frac{U(s)}{E(s)} = K_P \left[1 + \frac{1}{T_I s} \right] \quad (2.30)$$

2.5.5 Proportional-Differential (PD)

The PD-controller is the sum of the proportional and the differential controllers. A PD-controller is often adopted for an excitation control system [5]. The control law for the PD-controller is expressed in equation 2.31, while the transfer function is expressed in equation 2.32. The differential action in the system will always try to prevent the controlled variable to change, this will improve the system stability. At the same time if the differential time constant T_D is too large, the differential action will be too strong, which will influence the system stability.

$$u(t) = K_P \left[e(t) + T_D \frac{de(t)}{dt} \right] \quad (2.31)$$

$$G_c(s) = K_P \frac{T_D s + 1}{\frac{T_D}{K_D} s + 1} \quad (2.32)$$

2.5.6 Proportional-Integral-Differential (PID)

The PID controller is a combination of proportional-, integral- and derivative-control. It is most often used as a feedback controller, where it delivers the output at desired levels. If one want to use a proportional controller, or a PI-controller, one simply set the other parameters to zero. The expression of the transfer function of the PID control is as follows:

$$\frac{U}{\Delta U_i} = (K_p + K_D s) \frac{1}{1 + K_I s} \quad (2.33)$$

Where K_p , K_i and K_d are the proportional, integral and differential regulation factors, respectively.

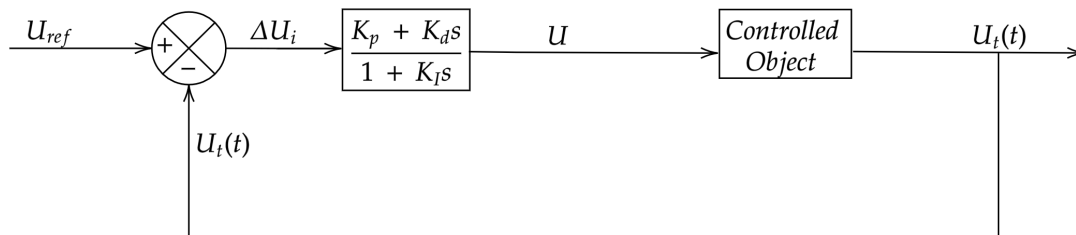


Figure 2.24: Block diagram of transfer function of a PID control.

3 Method

In this chapter, an excitation system for a SM is designed. The system will be based on a single-phase controlled rectifier, built up by thyristors, often termed SCR [22]. The SCR was chosen because of the need of a controllable rectifier, and its wide use in excitation systems [19]. The source of excitation power will be the single-phase AC power in the socket on the wall.

Matlab[®]/Simulink[®] is a commercial tool, which provides convenient solutions for system simulation technology [30]. Simulation studies comes with a couple of challenges. It can be hard to balance the system, so that it accounts for all physical phenomena that would occur in a physical model. Also systems which embrace multiple physical domains can come with some challenges. Matlab[®]/Simulink[®] along with Simscape Electrical[™], library used for all components, is both adressing these needs [31], [30].

3.1 Full[®]/Simulink[®] Model

Figure 3.1 display a sketch of the system designed in Matlab[®]/Simulink[®]. Full simulation is found in appendix B. The simulated model consists of a SM, excited by a controllable rectifier. Two control systems, are implemented for controlling the rectifier output, as well as the terminal voltage. The system consists of the following elements:

SM.	Modelled to behave as the Terco MV 1027-235 SM.
SCR bridge.	Single-phase controlled rectifier.
SCR control.	Controls the rectified DC voltage.
SM control.	Controls the terminal voltage of the SM.

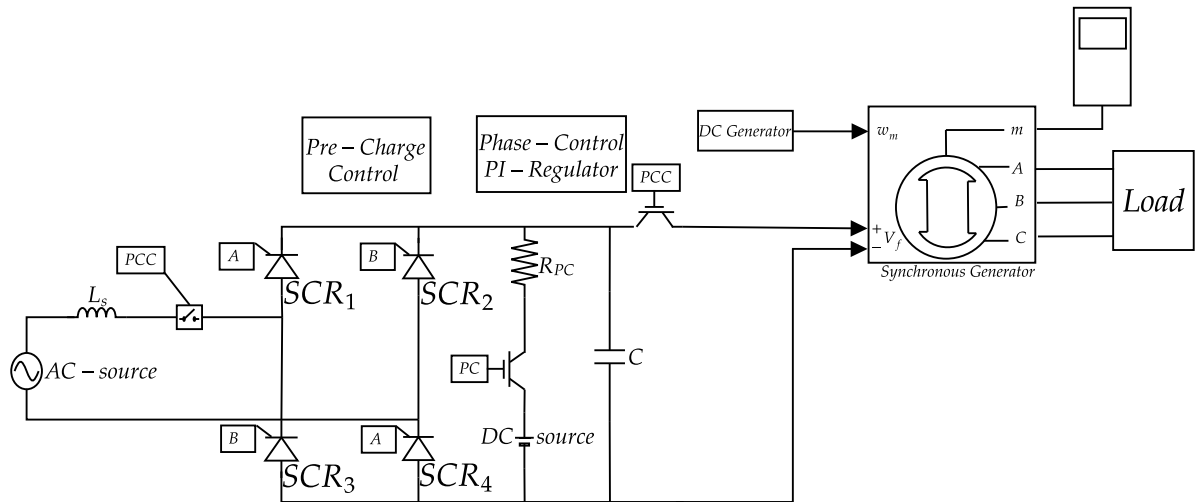


Figure 3.1: Sketch of Matlab®/Simulink® Model.

3.2 Synchronous Generator

The SM SI Fundamental block, from Simscape Electrical™, is used to simulate the generator of the system. It models a three-phase machine, with either round rotor or salient poles. The block uses parameters in SI units and can be driven as a motor or generator, depending on the mechanical input. The full block can be found in [32].

The machine is supposed to behave as the Terco MV1027-235 SM stationed at University of Bergen and Western Norway University. The datasheet for the Terco MV1027-235 can be found in appendix D.1. This is a small generator with a nominal power of 1.2 kVA, and the excitation source is set to 230 V AC Root Mean Square (RMS). A SCR-bridge is connected to the field winding of the machine, and will rectify the AC current into a controlled DC current. The parameters used in Matlab®/Simulink® is displayed in table 3.1.

Table 3.1: Parameters in Matlab®/Simulink® for the SM.

Parameters	Value	Description	Obtained from
P_N	1.2 kVA	Nominal power.	From ap. D.1
V_N	230 V	Nominal voltage	From ap. D.1
f_N	50 Hz	Nominal frequency	From ap.D.1
R_f	129.5Ω	Field resistance.	From [33].
L_f	7.7 H	Field inductance.	From [33].
R_s	1.4Ω	Stator resistance.	From [33].
L_{ssm}	25 mH	Stator inductance.	From [33].
L_{md}	1.2 H	Direct-axis mag. inductance.	Estimated.
L_{mq}	1.2 H	Quadrature-axis mag. inductance.	Estimated.

As the table displays, the parameters are collected both from the datasheet for the Terco MV1027-235 SM, previous tests on the machine and some are estimated.

3.3 SCR Bridge

The thyristor block, from Simscape Electrical™, is used to model the SCR. It represents a macro model of the real SCR, and does not account for the geometry or the complex physical processes. The macro model is simulated as a resistor, R_{on} , inductor, L_{on} , DC voltage source, V_f , and a switch connected in series.

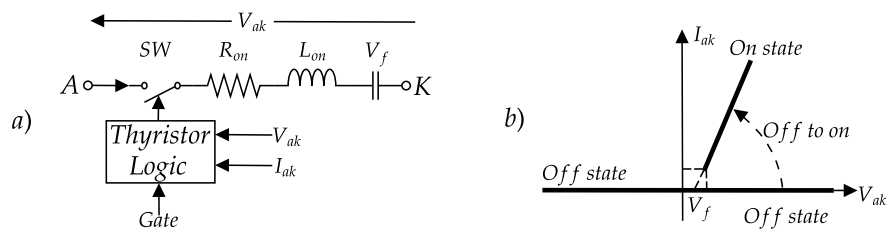


Figure 3.2: Thyristor block: a) Equivalen circuit b) VI characteristic.

Figure 3.2 a) displays the inside of the block. The block turns on via its gate, when a positive pulse signal is applied, given $V_{ak} > V_f$, and that the pulse last long enough so that I_{ak} becomes greater than I_l . It turns off when $I_{ak} = 0$ A, and a negative voltage, V_{ak} last equal or longer than the turn off time T_q .

A SCR is found for the system, so that practical parameters are implemented in the model. The parameters can be found in the datasheet, see appendix ??

Table 3.2: Parameters for SCR(Adapted from datasheet.)

Parameters	Value	Comment
R_{on}	0.001Ω	Internal resistance.
L_{on}	0 H	Internal inductance.
V_f	0.8 V	Forward voltage.
I_l	$80 \cdot 10^{-3}$ H	Latching current.
T_q	$100 \cdot 10^{-6}$ s	Turn-off time.
I_c	0 A	Initial current.
R_s	500Ω	Snubber resistance.
C_s	$250 \cdot 10^{-9}$ F	Snubber capacitance.

The bridge configuration and a pre-charge system is displayed in figure 3.3. The four SCRs work parallel to each other:

- SCR₁ and SCR₄. Rectifies the positive sinusoidal input voltage. Gate A.
 SCR₂ and SCR₃. Rectifies the negative sinusoidal input voltage. Gate B.

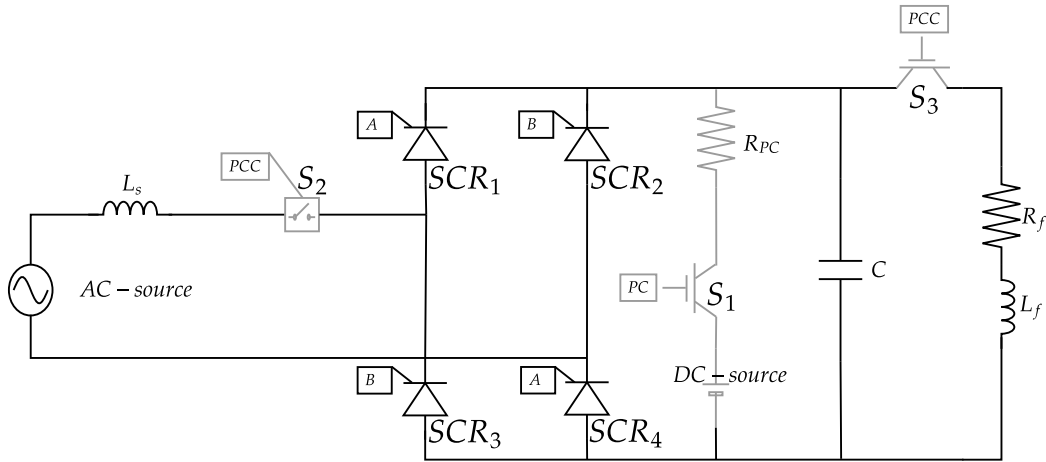


Figure 3.3: Topology of SCR bridge and pre-charge system.

Table 3.12 display the parameters for the different components in the bridge. Since the bridge is suppose to feed the field winding of the SM, the load resistor, R_L and load inductor, L_L is set equal to the field resistance, R_f and field inductor L_f , respectively. The voltage over R_L and L_L , represents the output voltage of the bridge. In Matlab[®]/Simulink[®] this voltage signal is measured, and sent to the SM. The current through this RL - load, has been measured and compared to the field current in the SM.

Table 3.3: Parameters for SCR bridge.

Parameters	Value	Comment
AC source	230 V AC 50 Hz	RMS value of input voltage.
L_s	1 mH	Source inductor.
C	50 mF	Smoothing capacitor.
R_L	129.5 Ω	Field resistance.
L_L	7.7 H	Field inductance.

3.4 Control Systems

Figure 3.6 display both the SCR control, and the terminal control, and the switching mechanism between them. They are both based on phase control for the SCRs. Phase control work by sending small pulses of current, to trigger the gates of the SCRs, and will stop conducting when the input voltage falls below the holding current, a term called natural commutation [34] [22].

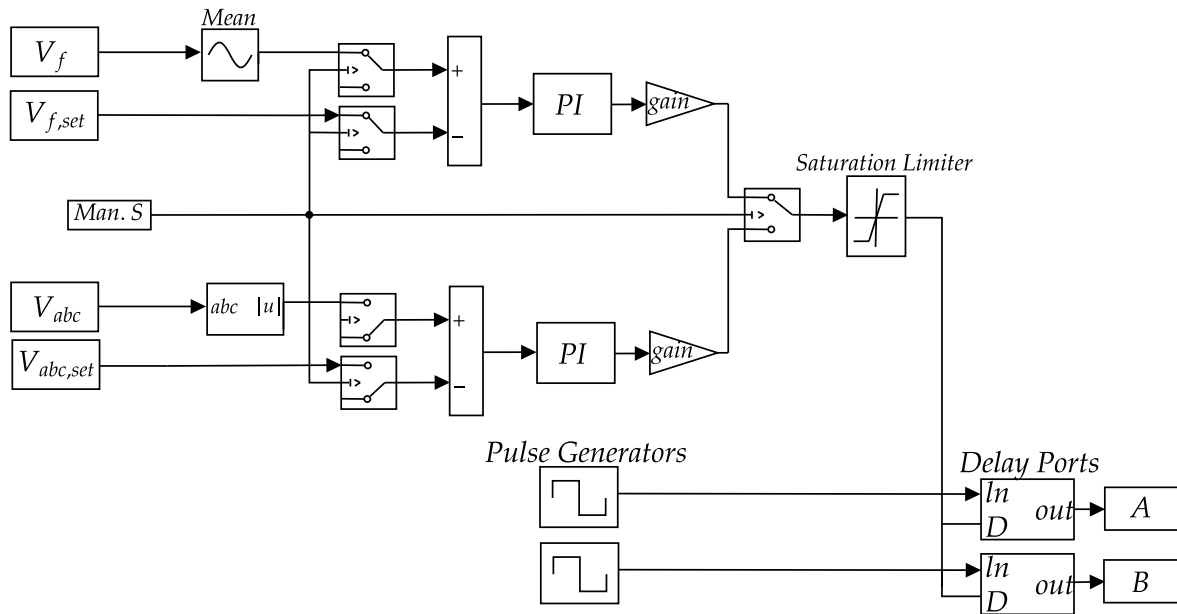


Figure 3.4: Sketch of full control system.

Table 3.4, show the parameters for the two pulse generators. The output of these blocks simulates the gate current which trigger the SCR pairs. The amplitude is set to one, and the period, T is calculated:

$$f = \frac{1}{T} \rightarrow T = \frac{1}{f} = 0.02 \tag{3.1}$$

Table 3.4: Parameters for pulse generator A

Pulse generator 1		Pulse generator 2	
Amplitude	1	Amplitude	1
Period	0.02 s	Period	0.02 s
Pulse width	30 %	Pulse width	30 %
Phase delay	0 s	Phase delay	0.01 s

The pulse width, tell us how long the signal lasts in % of the period. Both pulse generators, are firing one pair of SCR each. The only difference between the pulse generators, is the phase delay for the second one. These pulses are delayed by 0.01 s, which makes the second pair of SCRs, always lag behind by half a period and thus only conduct for the negative sinusoidal input voltage, and contrary the other pair will only conduct for the positive.

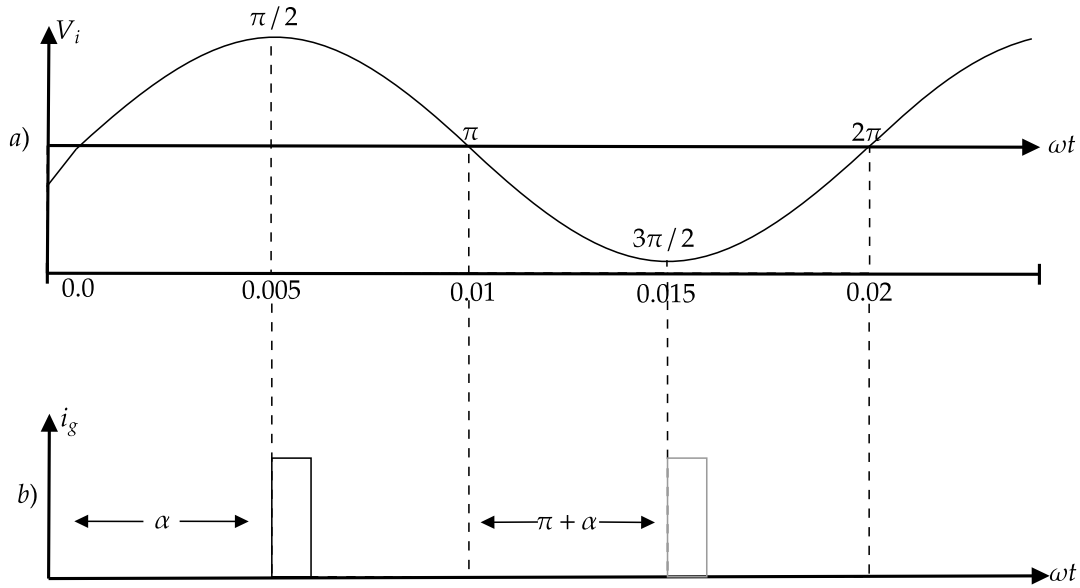


Figure 3.5: Sketch of: a) Input voltage b) Gate current

Figure 3.5, show that by delaying the gate current, the SCRs can be fired at desired angles of the input voltage. This angle is called the firing angle, α . By controlling the firing angle, the output is controlled.

3.4.1 SCR Control

The SCR bridge is controlled by a PI controller. The reason for not adding the derivative gain in the system, is from the fact that there were no significant difference whether it was added or not. Matlab[®]/Simulink[®] offers its own way of tuning the PI regulator. It is a model-based tuning method, which computes a linear model of the plant from the output and the input. This plant includes all of the blocks in the control loop, besides from the PI controller itself. Further on the tuner accumulate all of the input/output data by simulating the model over a short period of time, and both P and I is calculated. The parameters for the PI controller are displayed in table 3.5.

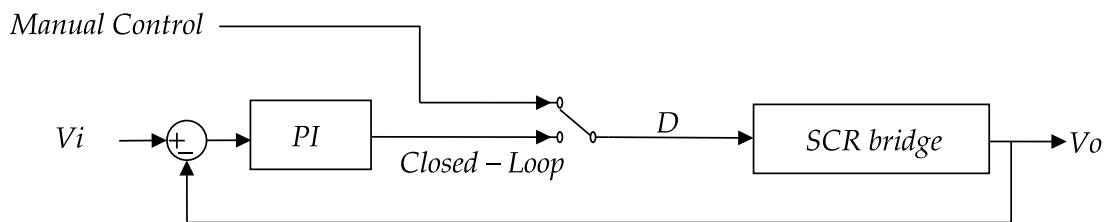


Figure 3.6: Sketch: Open VS Closed Loop for SCR control.

Table 3.5: Parameters for SCR bridge.

Parameters	Value
P	-0.08833
I	-0.07221

3.4.2 Terminal Control

The terminal control system, controls the three-phase output of the SM. Figure 3.7 show the block diagram of the system. The process represents the whole model. The amplitude of the three-phase output voltage, is measured and compared to the reference.

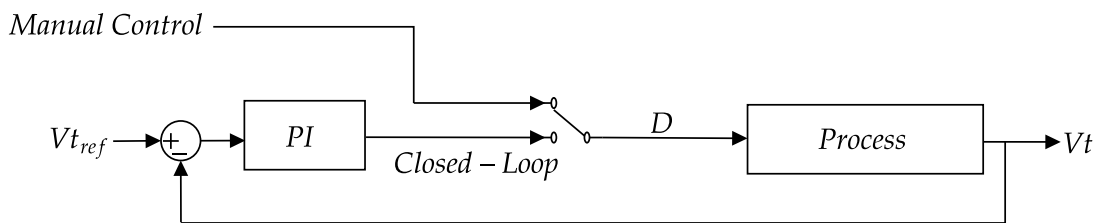


Figure 3.7: Sketch: Open VS Closed Loop for Terminal Control.

The PI parameters are displayed in table 3.6.

Table 3.6: Parameters for SCR bridge.

Parameters	Value
P	-0.0264
I	-0.00839

3.4.3 Pre-charge Control

The control of the pre-charge system is shown in 3.8. It is based on logic operators, and is made so that it will charge the capacitor to a desired value, before the bridge start its rectification. No pre-charge for the capacitor can lead to large inrush current, and by that the system will act as a protective circuit.

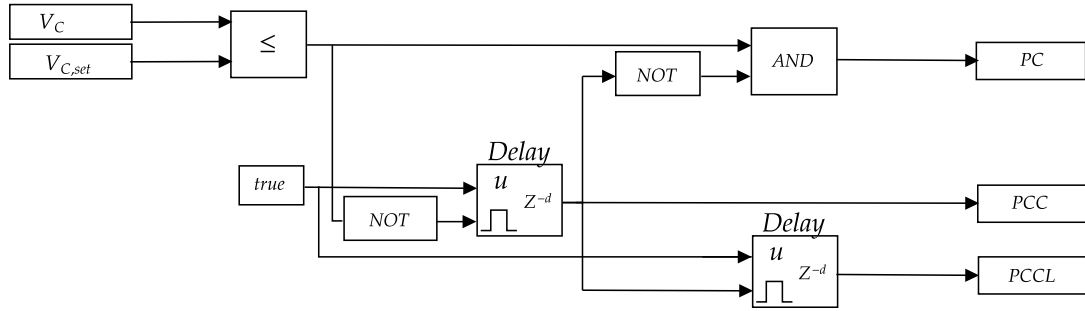


Figure 3.8: Control for the precharge system.

If the bridge is set to start at a desired output voltage, the DC source is set equal, so that the system will charge the capacitor before the system starts running. In theory, the SCR bridge could run without a pre-charge, since it is in fact controllable. On the other hand, from a practical perspective, pre-charge of the capacitor should be implemented.

Table 3.7: Parameters for SCR bridge.

Parameters	Value	Comment
DC source	V_{DC}	Set to the desired capacitor voltage.
R_{PC}	1 mH	Source inductor.
C	50 mF	Smoothing capacitor.
R_L	129.5 Ω	Field resistance.
L_L	7.7 H	Field inductance.

3.5 Step Response SCR Bridge

A dynamic response is done on the SCR bridge, to find the 1.order transfer function.

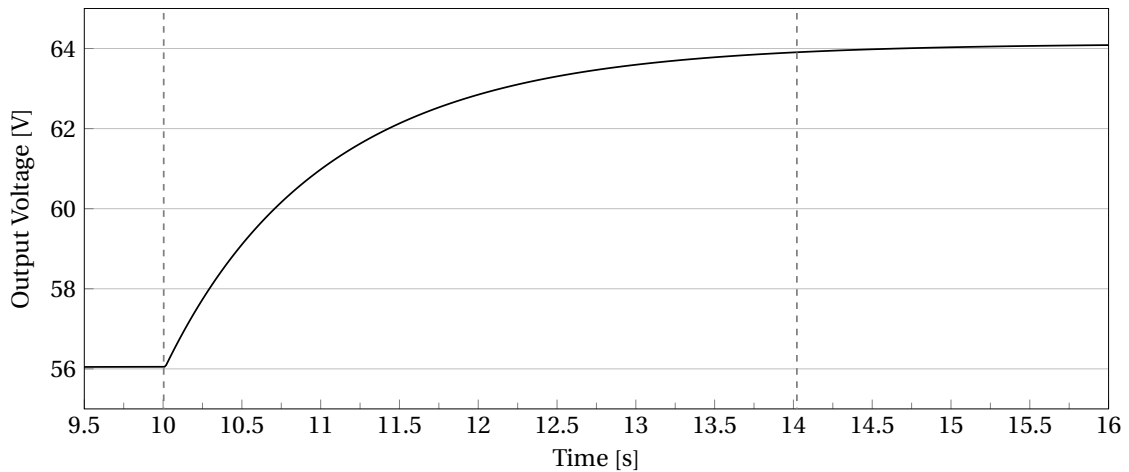


Figure 3.9: Step response for SCR bridge.

Table 3.8: Dynamic response on the terminals.

Output voltage	Time	Delay
$V_o = 56.05 \text{ V}$	$t_1 = 10.004 \text{ s}$	$D_0 = 0.009$
$V_{of} = 63.91 \text{ V}$	$t_2 = 14.022 \text{ s}$	$D_f = 0.0089$
$\Delta V_o = 7.86 \text{ V}$		$\Delta D = -1.0 \cdot 10^{-4}$

The gain and time coefficient for the 1.order system, is calculated in equation 3.2 and 3.3 respectively.

$$K = \frac{\Delta V_o}{\Delta \alpha} = -1.2723 \cdot 10^{-5} \quad (3.2)$$

$$V_{t63\%} = V_o + 63\% \cdot \Delta V_o = 61.0018\text{V} \rightarrow T = 2.9540 \text{ s} \quad (3.3)$$

The first order transfer function for the SCR bridge is expressed in equation 3.7.

$$G_{aut} = \frac{K}{Ts + 1} = \frac{-1.272 \cdot 10^{-5}}{2.954s + 1} \quad (3.4)$$

3.6 Step Response Full Process

A dynamic response is done for the terminal control system, to obtain the transfer function of the full process. The input delay variable was set to a value that corresponded to 200 V on the terminal. The delay were then applied a step so that the output rised to a new value. Figure 3.10 displays the response on the terminals. Full calculations are shown in appendix (WILL AD).

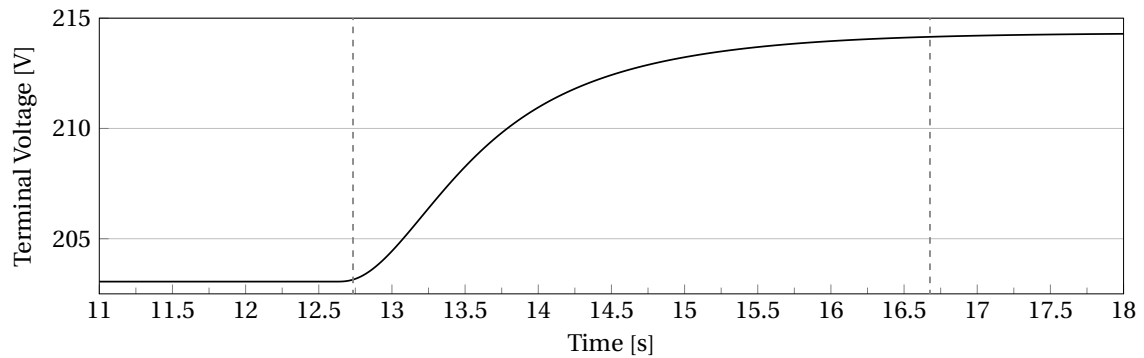


Figure 3.10: Dynamic response test to find the 1.order transfer function for the system.

Table 3.9: Dynamic response on the terminals.

Terminal Voltage	Time	Delay
$V_{t0} = 203.1 \text{ V}$	$t_1 = 12.734 \text{ s}$	$D_0 = 0.0086$
$V_{tf} = 214.2 \text{ V}$	$t_2 = 16.677 \text{ s}$	$D_f = 0.00855$
$\Delta V_t = 11.1 \text{ V}$		$D = -5 \cdot 10^{-5}$

The gain and time coefficient for the 1.order system, is calculated in equation 3.5 and 3.6 respectively.

$$K = \frac{\Delta V_t}{\Delta D} = -4.5045 \cdot 10^{-6} \quad (3.5)$$

$$V_{t63\%} = V_{t0} + 63\% \cdot \Delta V_t = 210.093 \text{ V} \quad \rightarrow \quad T = 2.667 \text{ s} \quad (3.6)$$

The first order transfer function for the automatic control system is found in equation 3.7.

$$G_{aut} = \frac{K}{Ts + 1} = \frac{-4.5045 \cdot 10^{-6}}{2.667s + 1} \quad (3.7)$$

3.6.1 Additional PI-Tuning for Terminal Control

The Ziegler-Nichols and Cohen-Coon tuning methods will also be tested on the automatic regulator, and compared against the regulator tuned in Matlab[®]/Simulink[®]. These methods are based on the reaction curve found by the open loop experiment. The input that controls the system, is forced to a desired value, and applied a step. The output is measured and the reaction curve can be obtained. The PI parameters can then be calculated from the tables found in appendix C.

Table 3.10: Readings for figure 3.11

Terminal Voltage	Time	Delay
$V_{t0} = 203.1 \text{ V}$	$t_0 = 12.61 \text{ s}$	$D_0 = 0.0086 \text{ s}$
$V_{tf} = 214.2 \text{ V}$	$t_1 = 12.84 \text{ s}$	$D_{0f} = 0.00855 \text{ s}$
$\Delta V_t = 11.1 \text{ V}$	$t_2 = 14.25 \text{ s}$	$\Delta D_0 = -5 \cdot 10^{-5} \text{ s}$

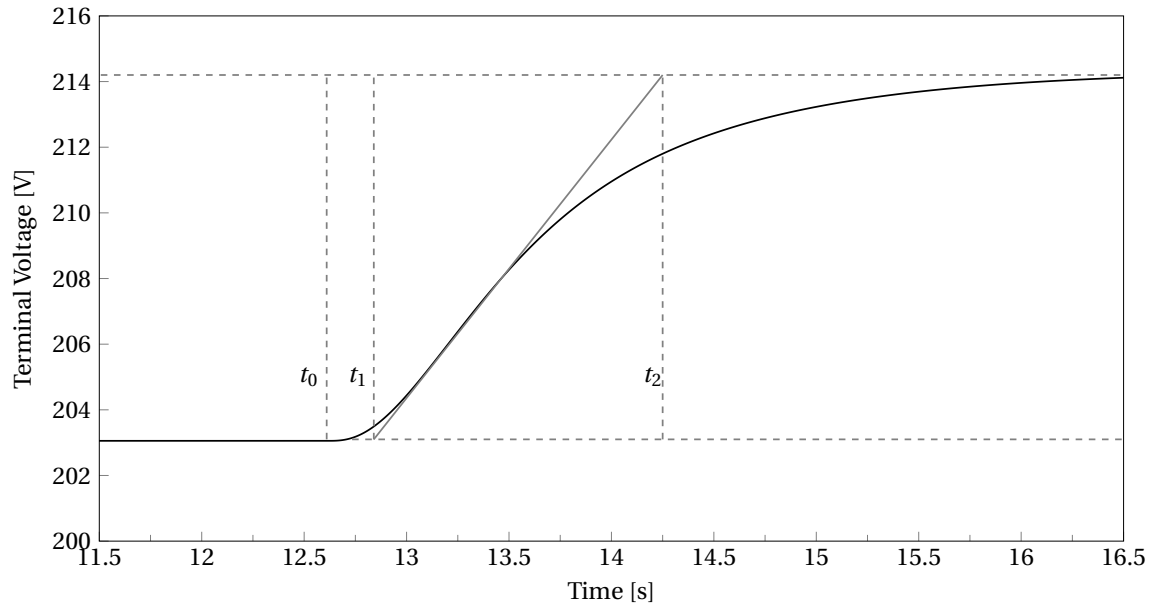


Figure 3.11: Reaction Curve.

$$K_{pZiegler-Nichols} = \frac{0.9v_0}{K_0\tau_0} = 2.3842 \quad T_{rZiegler-Nichols} = \tau_0 = 0.273 \quad (3.8)$$

Table 3.11: Parameters for Ziegler-Nichols tuned regulator.

Parameters	Value
P	$-2.4853 \cdot 10^{-5}$
I	$-3.6019 \cdot 10^{-5}$

Table 3.12: Parameters for Cohen-Coon tuned regulator.

Parameters	Value
P	$-2.5228 \cdot 10^{-5}$
I	$-4.4115 \cdot 10^{-5}$

4 Results

The tests have been done while the generator has been in an open-circuit condition. This condition has been simulated by a very low load, so that approximately no current was drawn. The mechanical input has been set at a constant at 1500 RPM, so that the terminals produce 50 Hz. The results will be presented in the same order, as the method has presented the system.

4.1 SM Input/Output

This section shows the mechanical input, the field voltage and the terminal voltages, shown in figure 4.1, 4.2 and 4.3, respectively. The period in each sinusoidal voltage was measured to 20 ms which proves that the frequency on the terminal is 50 Hz, see 3.1. This is a result of the machine having 2 poles and the mechanical input set to 1500RMS, see equation 2.1.

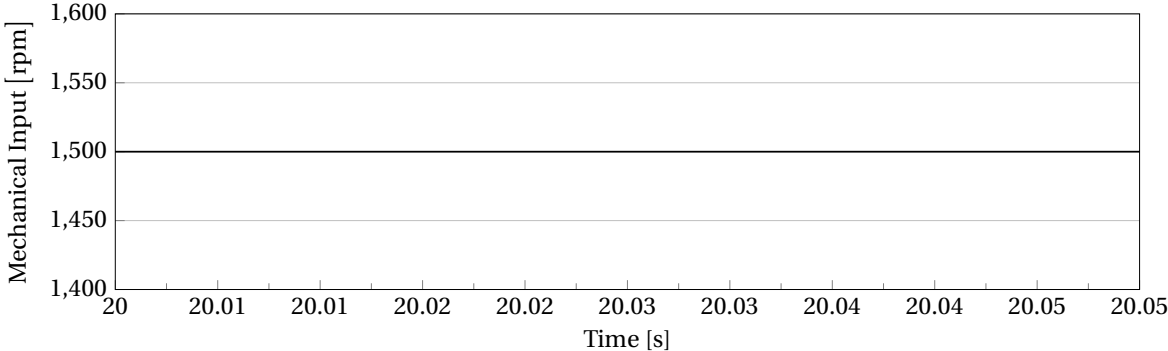


Figure 4.1: Constant mechanical input at 1500 RPM.

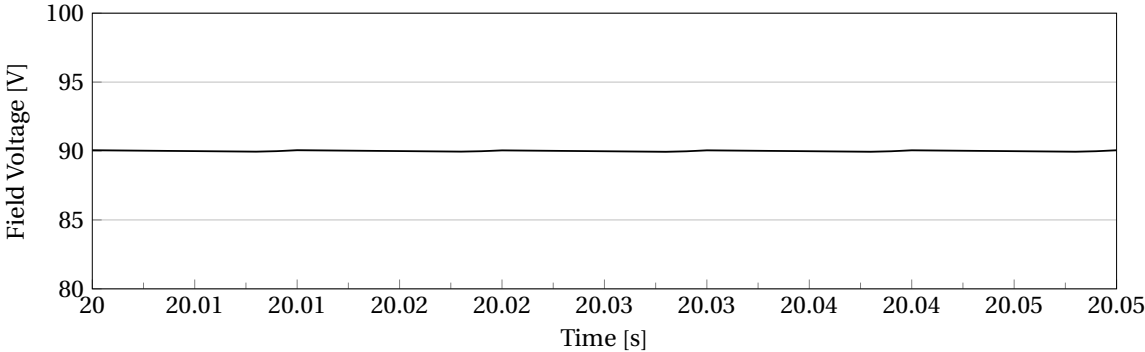


Figure 4.2: Field voltage set at a reference of 90 V.

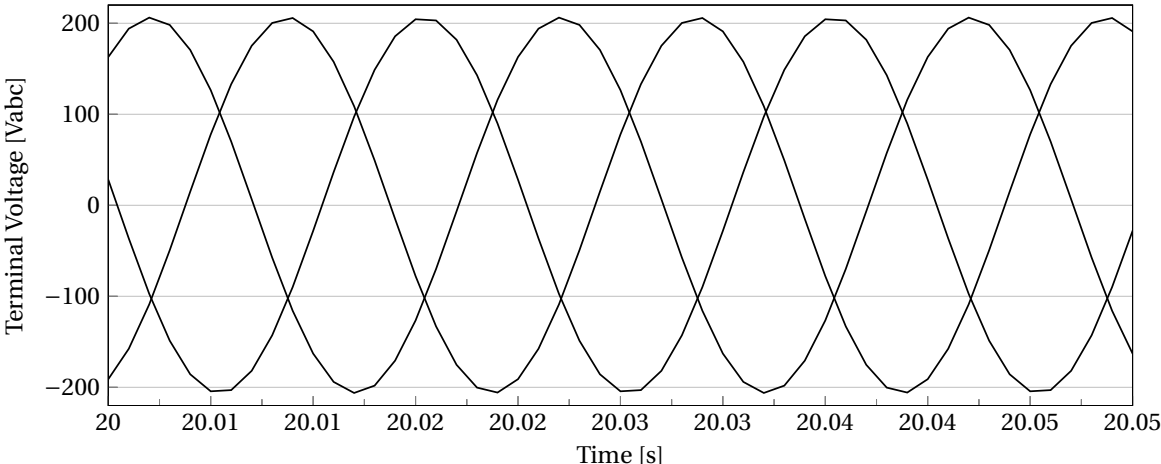


Figure 4.3: V_a, V_b and V_c as a result of the mechanical input and the field voltage.

4.2 Relationship between i_f and V_t

Figure 4.4 shows the relation between the field current and the peak value of the terminal voltage. The designed system is simulated with no saturation. The stippled line in the figure display the magnitude of the field-current, measured to 0.673 A, when the peak of the terminal voltage is 200 V.

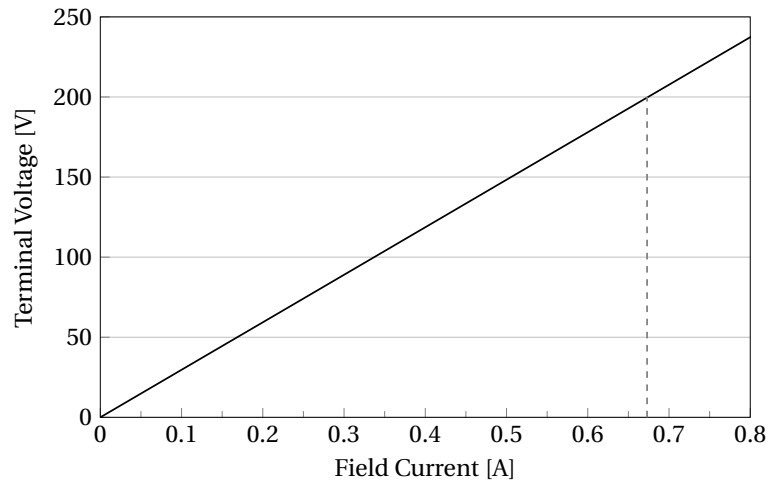


Figure 4.4: Relationship between Field Current and Terminal Voltage.

4.3 Bridge Output

In this section the SCR bridge is tested in an open loop condition. The delay, or the firing angle, α , is set to fixed values.

Figures 4.5, 4.6 and 4.7 show the input voltage, output voltage, and the two gate currents that are sent to the SCR pairs. The delay is fixed so that the firing angle, $\alpha = 180^\circ$, and this gives zero voltage output as expected, see figure 4.6.

Similarly, figures 4.8, 4.9 and 4.10, show the input voltage, output voltage, and the two gate currents when the delay gives firing angle, $\alpha = 0^\circ$. This gives the maximum output of 310.9 V DC, displayed in figure 4.9. Figure 4.10 shows that the gate currents are now firing the SCRs so that they conduct for the entire sinusoidal input wave.

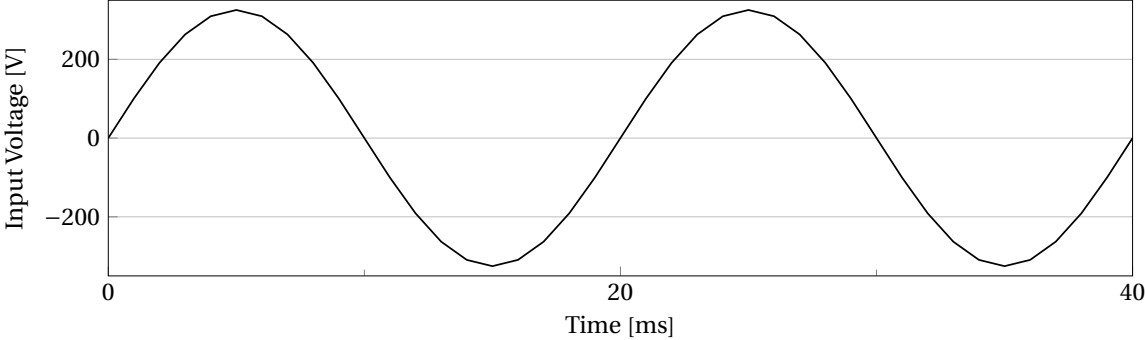


Figure 4.5: Input voltage over a period of 40 ms, and $\alpha = 180^\circ$.

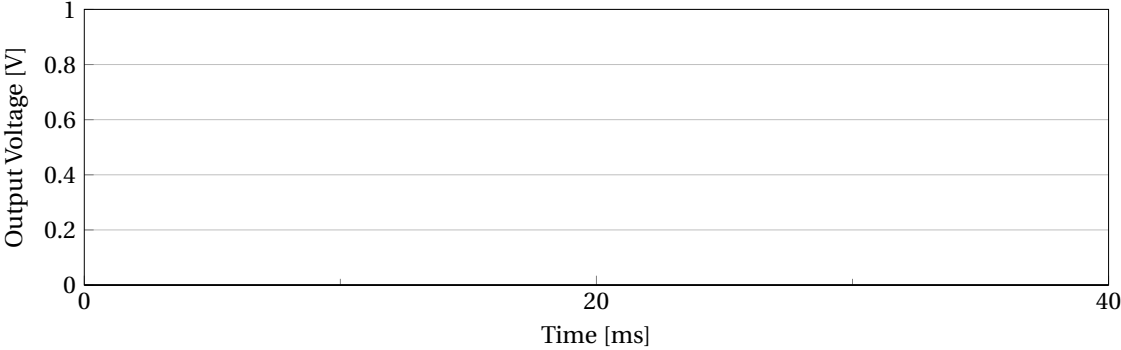


Figure 4.6: Output voltage over a period of 40 ms, and $\alpha = 180^\circ$.

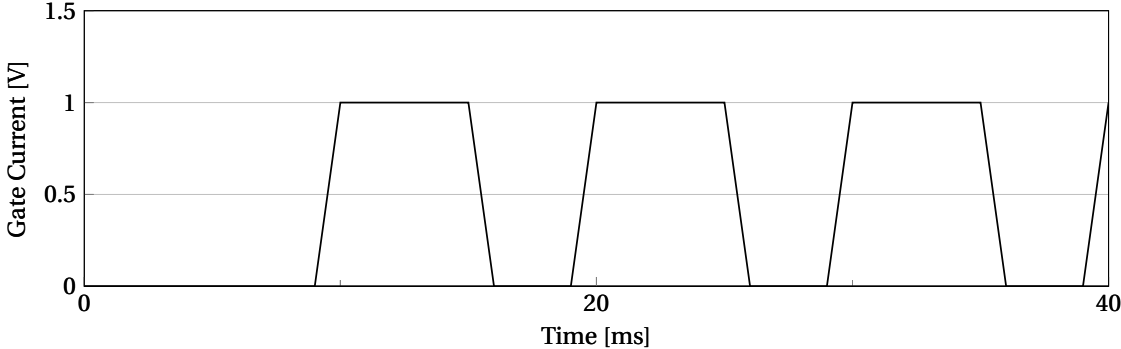


Figure 4.7: Gate currents over a period of 40 ms, and $\alpha = 180^\circ$.

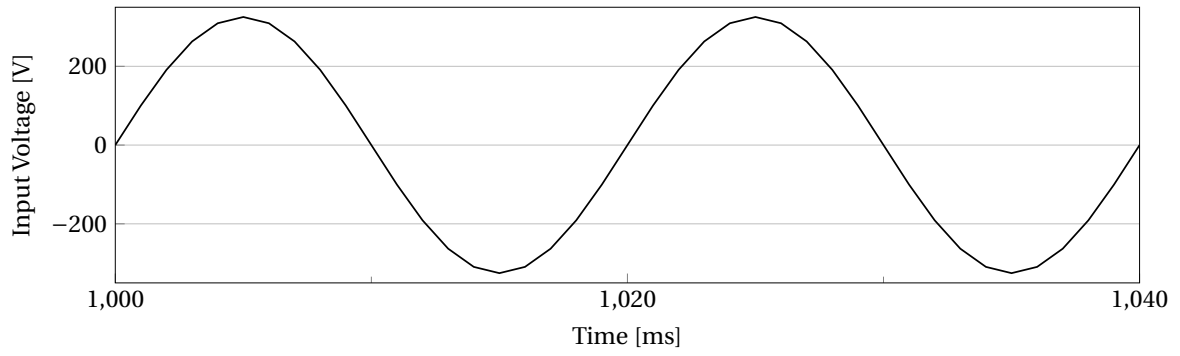


Figure 4.8: Input voltage over a period of 40 ms, and $\alpha = 0^\circ$.

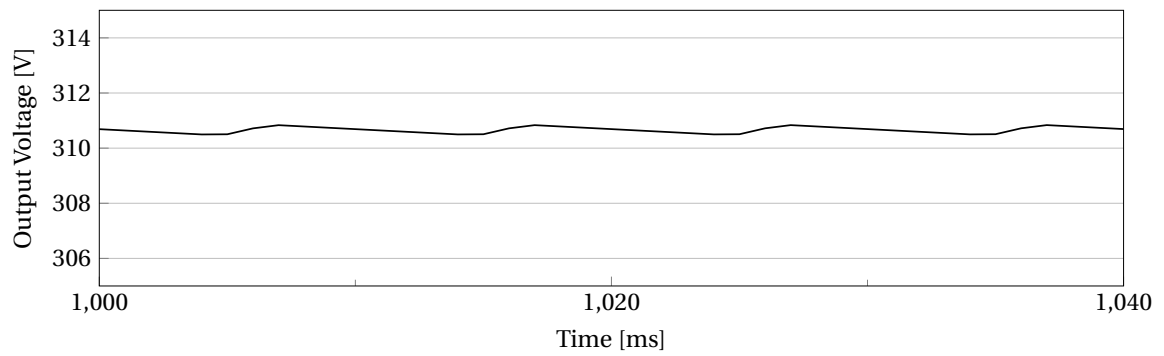


Figure 4.9: Output voltage over a period of 40 ms, and $\alpha = 0^\circ$.

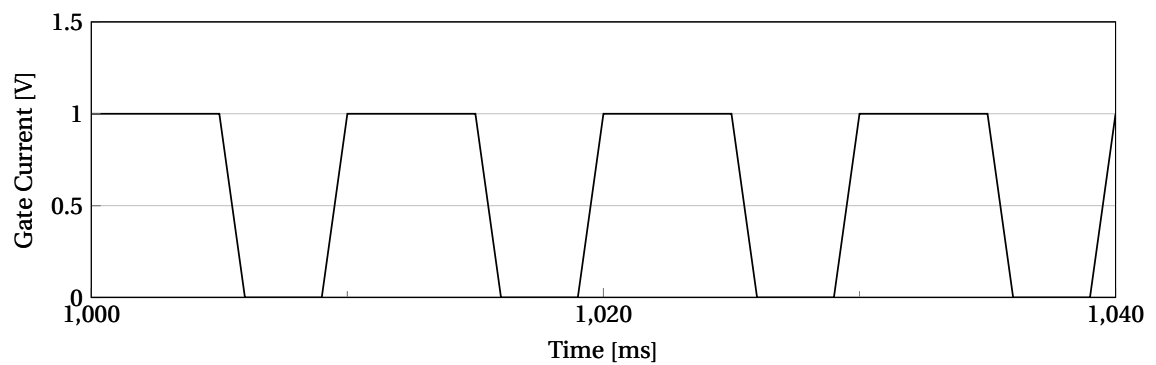


Figure 4.10: Gate currents over a period of 40 ms, and $\alpha = 0^\circ$.

4.4 SCR Control

Figures 4.11 and 4.11, show how the voltage is stepped up to a desired voltage. The system is in this state controlling the output of the rectifier, and hence the field voltage for the machine. The voltage is stepped up in steps of 15 V until 90 V is reached, see figure 4.11. This gives a peak-value of 206.3 V on the terminals as shown in figure 4.12.

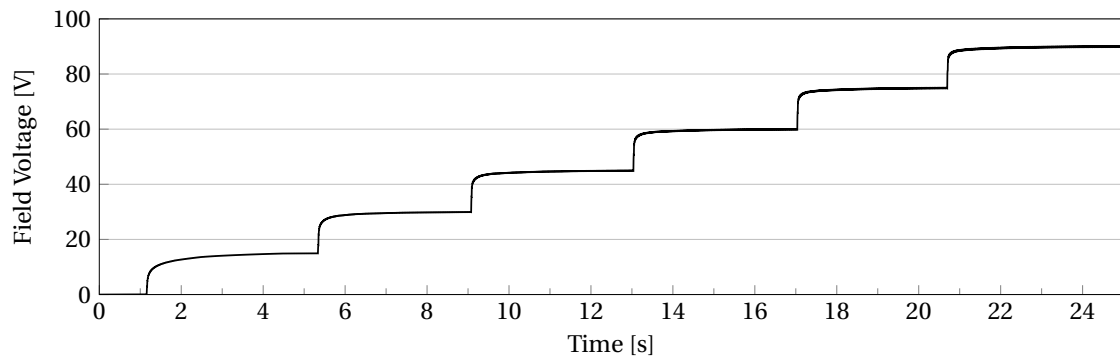


Figure 4.11: Field voltage step up, 15 V each step.

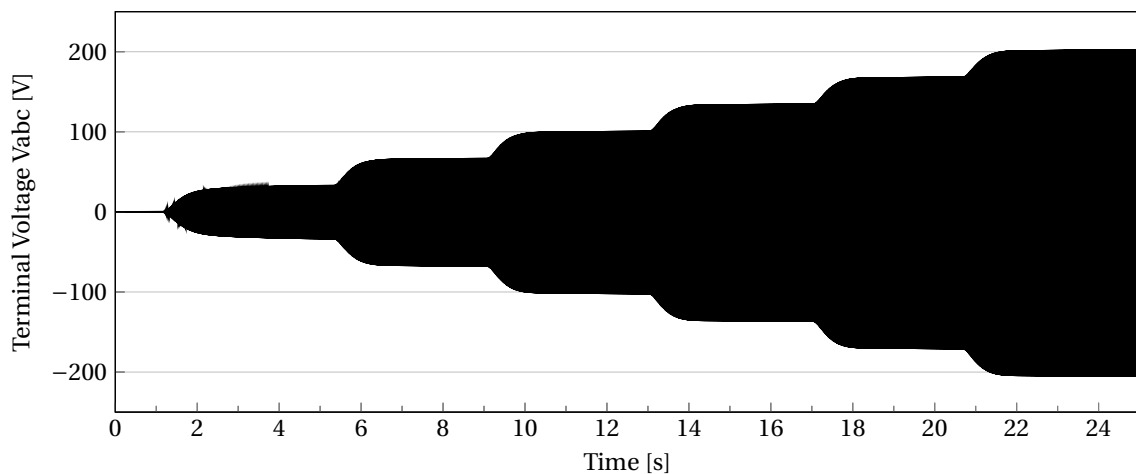


Figure 4.12: Voltage step up on the terminal of the machine.

Throughout this test the current through SCR_1 , is measured and shown in figure 4.13. The peak of the current, is a inrush current that occurs, when the voltage is stepped up. The voltage were stepped up in steps of 15 V, and the figure represents the highest one that occurred.

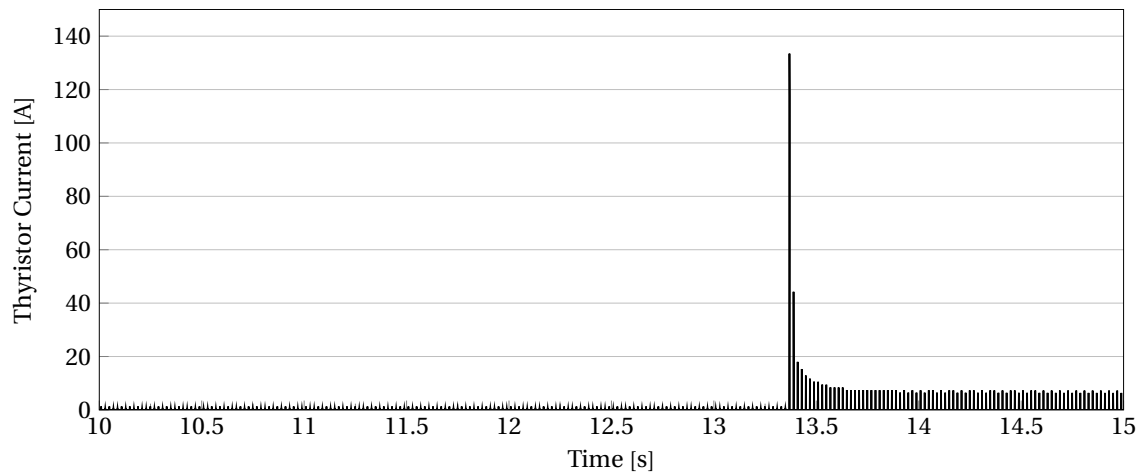


Figure 4.13: The current through SCR₁ while stepping up the voltage in steps of 15 V.

4.5 SCR to Terminal Control

The SCR control is set to hold the peak of the terminal voltage at a reference of 200 V peak-value. The system is still connected to a very low load, to simulate open-circuit conditions, so that the load draws approximately zero current. Figures 4.14 and 4.15 show the field and terminal voltage, and their variations, respectively. The field voltage is stepped up to 90 V, and stabilized before the switching are done. Shown in section 3.6, the peak value of the terminal voltage is stabilized at 206.3 V with a field voltage of 90 V, and when the terminal voltage is set to 200 V the figures show how the field voltage is stabilizing at around 87.3 V.

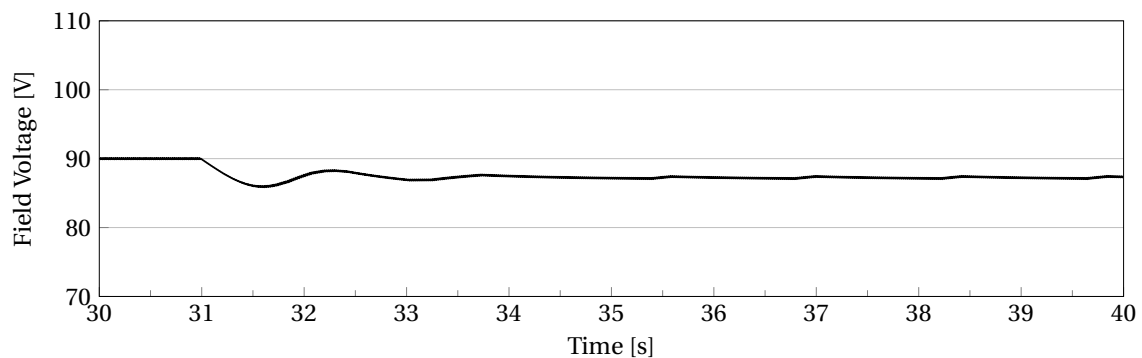


Figure 4.14: Field voltage variations, switching from SCR to terminal control.

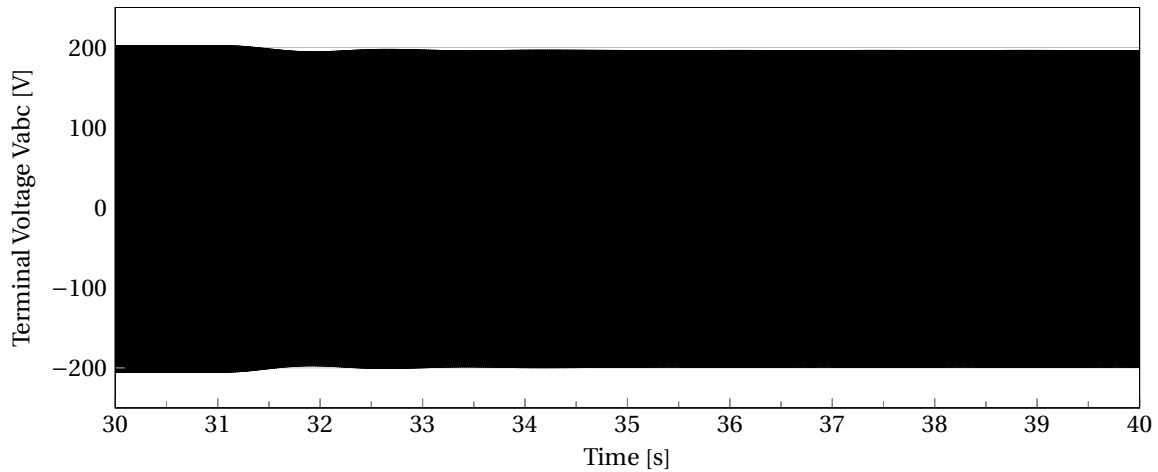


Figure 4.15: Terminal voltage variations, switching from SCR to terminal control.

4.6 Mechanical Input Variations

Some mechanical input variations are done while the system is in the state of automatic control. The control system is still set to hold the peak value of the terminals at 200 V. This test shows how the control systems respond when the RPM first drops, and then rises again.

Figures 4.16 and 4.17 again show the field and terminal voltages. The system is here dropped at a constant speed of 1500 RPM to 1400 RPM in a step, and the figures show how the voltages respond. As figure 4.16 shows, the field voltage increases from 87.3 V to approximately 93.6 V.

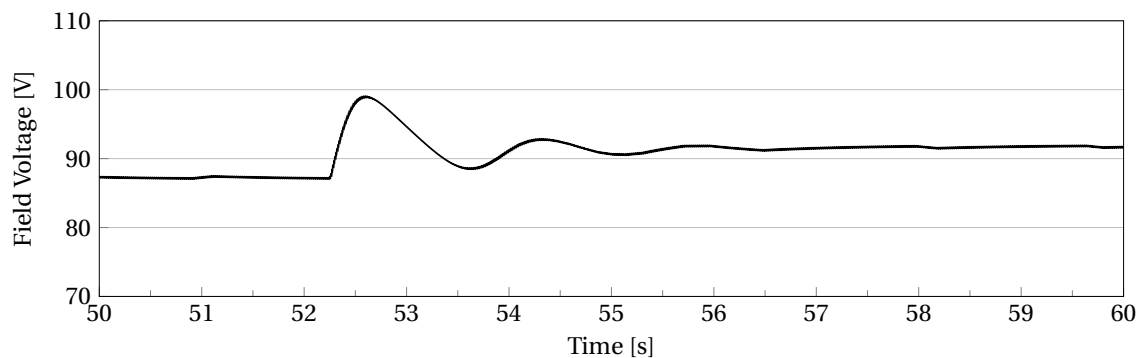


Figure 4.16: Field voltage response from decreasing the mechanical input to 1400 RPM.

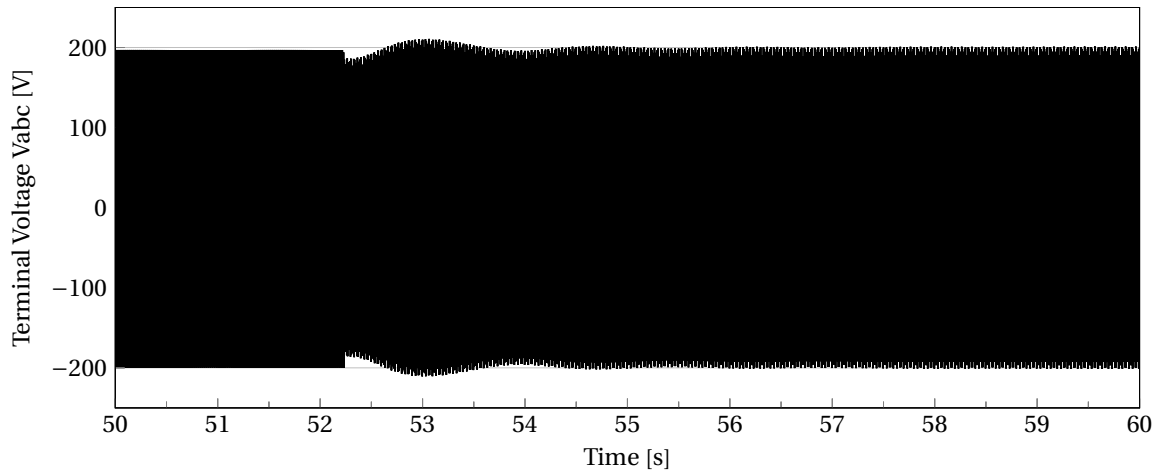


Figure 4.17: Terminal voltage response from decreasing the mechanical input to 1400 RPM.

Figures 4.18 and 4.19 show the field and terminal voltages, when the system increases the mechanical input as a step from 1400 RPM to 1500 RPM. The field voltage is now decreasing from 93.6 V back to 87.3 V.

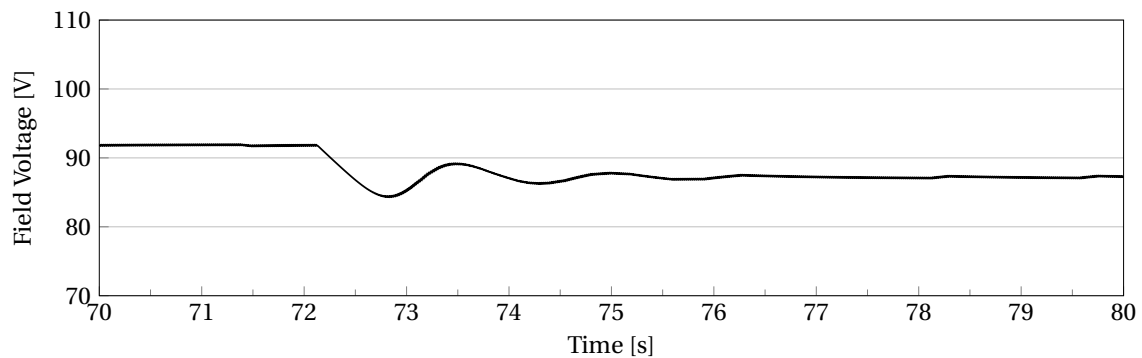


Figure 4.18: Field voltage response from increasing the mechanical input to 1500 RPM.

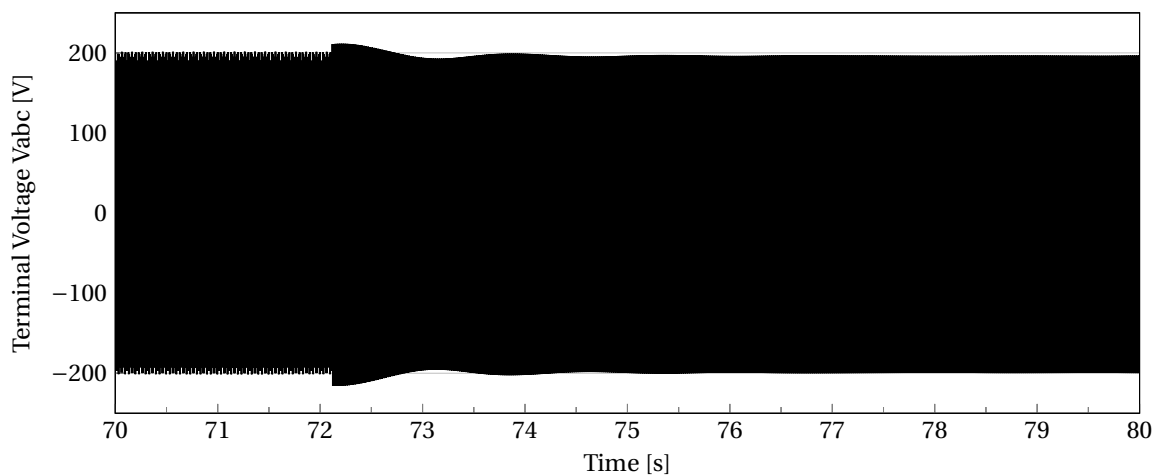


Figure 4.19: Terminal Voltage response from increasing the mechanical input to 1500 RPM.

4.6.1 PI Comparison

In this section the Ziegler-Nichols and Cohen-Coon PI tuning are used and compared against the autotuned PI regulator. All measures has been done at the exact same moment for all of the controllers, so that they could easily get compared.

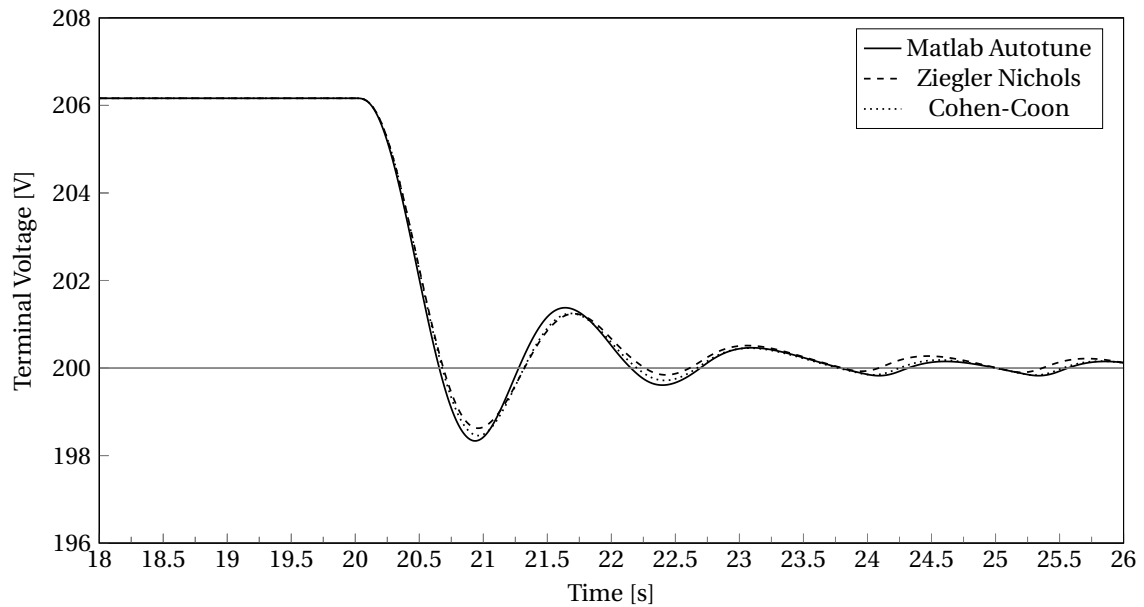


Figure 4.20: Switching from SCR control to terminal control.

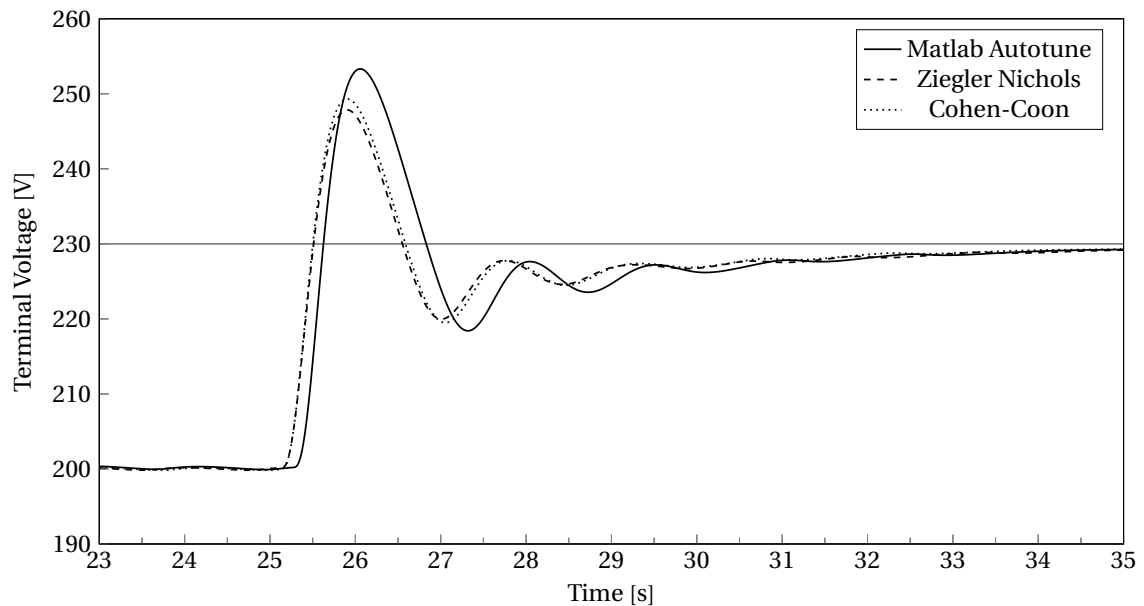


Figure 4.21: Reference change from 200 V to 230 V.

5 Discussion

The excitation system plays an essential role in the stability of modern power systems. They have received a lot of protective and control functions that result in a more stable system. The main goal of this thesis was to look into the existing excitation systems out there and design an excitation system for a small synchronous generator. The SM, stationed at the Western Norway University of Applied Science, parameters has been used to make the simulated SM, designed in Matlab[®]/Simulink[®], to behave the same.

The excitation system design can come close to a Type AC system, since a single-phase AC source is used as the excitation source. Further more a SCR bridge rectifier was chosen to, rectify the AC current into DC current. This choice was made because of the need of a controlled rectifier and that most literature used SCRs for this purpose.

The rectifier was analyzed by forcing the delay, and hence the firing angle, α to some desired angles. Section 4.3 showed that when the firing angle α is set to 180° , the output of the bridge reached to $0V$. That shows that the SCRs are blocking for the whole sinusoidal AC input. The maximum output was achieved at α equal to zero degrees, and the maximum voltage was measured at approximately $310.9V$.

This show that the bridge manage to control voltages as high as the maximum excitation voltage that the Terco MV1027-235 can handle, that is $220V$, as shown in the datasheet in appendix D.1. The saturation limiter can then be programmed, so that the bridge will never let through more excitation power then the SM can handle.

To get the output of the bridge, the field voltage, to start at zero voltage output, the PI controller for the bridge controller, were given an initial value that correspond to the firing angle α equal to 180° . Figure 4.7 show that the firing pulses are shifted 180° . For the automatic control system, the PI controller got an initial value corresponding to the reference terminal peak voltage at $200V$ AC. This make the switching, from bridge controller to automatic controller, more smooth bigger overshoots avoided.

The designed SM were simulated to behave as the Terco MV1027-235 as much as possible. Parameters used in the simulation were found from the datasheet and results from former

students, as shown in appendix D.1. By constant mechanical input of 1500 RPM, 50 Hz on the terminals were achieved, as shown in figure 4.3. The relationship between the field voltage and the peak terminal voltage of the simulated machine, is not quite similar to the actual machine. Studying the open circuit test, see [33], the simulated SM got a slight higher ratio between the voltages. This is probably a result of the estimations of the parameters, L_{md} and L_{mq} .

The relationship between the field current and the terminal voltage is displayed in figure 4.4. This figure shows how the peak voltage on the terminals increases with the field current and shows the field current when the system is running at reference terminal voltage at 200 V. The generator is simulated without taking the saturation into account. In a real generator, the field flux will increase linearly with the field current until a certain point, but the terminal voltage will start to degrade when the machine is overexcited. Since the SM operates way below the maximum field current given in the datasheet, the saturation is not accounted for.

The bridge controller is designed to control the output voltage of the bridge to desired values. In this manner, the user can set the field voltage to desired values. A PI controller was used in series with a saturation limiter so that the firing of the SCRs would always happen within its limits. A flowchart was implemented in Matlab[®]/Simulink[®], that delayed each step by 0.25 s. In this way, the inrush-currents over the thyristors got minimized and, in that manner, protect them. The highest inrush current that was measured when the field-voltage stepped up to 90 V, is shown in figure 4.13. This inrush-current was measured to approximately 141.2 A. This should not be a problem for the SCRs because of their high power handling capabilities.

The switching from controlling the bridge to controlling the terminals, happens after the desired field voltage is reached. As figure 4.14 shows, the system spends a few seconds to stabilize. The terminal voltage drops from 206.3 V AC peak, to 200 V AC peak, as shown in figure 4.15. These results show that the PI controller overshoots a bit when the systems are switched, but not very much. This could probably be fixed by tuning the PI controller even better, but the terminals are staying between the $\pm 10\%$ of the reference voltage. Hence, they follow the Norwegian standard, written about in chapter 1. Also, tests, which the RPM varied were executed to see how the control system reacts. The system was both exposed by decreasing the mechanical input from 1500 RPM to 1400 RPM, and vice versa. The results show a bit overshoot coming from the PI controller. Still, one could argue that in real life, the mechanical input would never drop or increase by 1000 RPM at an instance of time, and hence, the control system would get a bit more time to adjust both on the increase, and decrease, of the mechanical input.

Three different PI controllers got tested on the automatic control system. These are all compared in figure 4.20, where the control is switched from controlling the SCR to controlling the

terminals. In figure 4.21, they have all stabilized and applied a step. The results show that the calculated PI parameters perform as good, or if not better then the autotuned parameters. The Ziegler-Nichols and Cohen-Coon both responds quicker and shows less overshoot.

Generally the control system is pretty slow. This is because of the slow switching mechanisms that comes with the SCR, and by using some other switches the system could be made faster.

6 Conclusions

Design of an excitation system for a SM was investigated and presented in this thesis. A rectifier based on SCRs worked as the exciter, which rectified the AC current and fed the SM with DC current to magnetize the field winding of the machine. Therefore, this excitation system could be classified as an AC excitation system, based on the source of excitation. A control system to regulate the output voltage of the SCR was developed. This system makes it possible to control the field voltage directly, and step it up to a desired value. An automatic control system was also developed which controlled the terminal voltage output of the SM. Both control systems, were based on controlling the firing angle α , by the means of phase control, for the SCR bridge, and both seemed to work fine when exposed with different tests. A comparison between the Ziegler-Nichols and Cohen-Coon tuning method, and the auto-tuning implemented in Matlab[®]/Simulink[®] was performed and shows pretty similar results. The thesis has covered a wide range of topics, all the way from control systems, power electronics, excitation systems and the SM itself. It provides information about the most essential components and systems evolving the excitation system. The work did result in a working excitation system in Matlab[®]/Simulink[®], which could be implemented in future projects. It can however be challenging to balance the simulation, in the manner of including all physical phenomena, and contrary not make it too complex for practical applications. The simulation has included parameters from different datasheets, and components, that are used in practical applications, accounting for some of these challenges.

Future Work

The simulated SM could be optimized by more exact parameters.

- The control system proves to be functional, but could be improved by more advanced control loops.
- Implement the system in the laboratory. Proposed component list can be found in appendix C.
- Implementation of control units, described in section 2.4.

References

- [1] A. Bergen and V. Vittal, *Power Systems Analysis*, en, Second, ser. 2. United States of America: Tom Robbins, 2000, vol. 2, ISBN: 0-13-691990-1.
- [2] Z. Guan, X. Wang, X. Bian, L. Wang, and Z. Jia, "Analysis of causes of outdoor insulators damages on HV and UHV transmission lines in China," en, in *2014 IEEE Electrical Insulation Conference (EIC)*, Philadelphia, PA, USA: IEEE, Jun. 2014, pp. 227–230, ISBN: 978-1-4799-2789-0 978-1-4799-2787-6 978-1-4799-2786-9. DOI: 10.1109/EIC.2014.6869381.
- [3] Y. Qun and G. Jianbo, "Self-organized Criticality and Its Application in Power System Collapse Prevention," en, in *2006 International Conference on Power System Technology*, Chongqing, China: IEEE, Oct. 2006, pp. 1–3, ISBN: 978-1-4244-0110-9 978-1-4244-0111-6. DOI: 10.1109/ICPST.2006.321740.
- [4] J. Hauer, N. Bhatt, K. Shah, and S. Kolluri, "Performance of "WAMS East" in providing dynamic information for the North East blackout of August 14, 2003," en, in *IEEE Power Engineering Society General Meeting, 2004.*, vol. 2, Denver, CO, USA: IEEE, 2004, pp. 1685–1690, ISBN: 978-0-7803-8465-1. DOI: 10.1109/PES.2004.1373161.
- [5] J. Li, *Design and Application of Modern Synchronous Generator Excitation Systems*, en. John Wiley & Sons, Jun. 2019, ISBN: 978-1-118-84087-0.
- [6] Olje og energidepartementet, "Forskrift om leveringskvalitet i kraftsystemet - Lovdata," lovdata, Dec. 2004.
- [7] Kundur, *Power System Stability And Control*, en. McGraw-Hill, 1994, ISBN: 978-0-07-063515-9.
- [8] A. E. Fitzgerald, C. Kingsley, and S. D. Umans, *Electric Machinery*, en, 6th ed, ser. McGraw-Hill Series in Electrical Engineering. Boston, Mass: McGraw-Hill, 2003, ISBN: 978-0-07-366009-7 978-0-07-112193-4.
- [9] R. Hongtao, "Analysis of the Short Circuit at the Outlet of Self-excited Synchronous Generator," en, p. 4,
- [10] "IEEE Std 421.5™-2016 (Revision of IEEE Std 421.5-2005)," en, p. 207, 2016.

- [11] W. Wright, R. Hawley, and J. Dinely, "Brushless Thyristor Excitation Systems.," en, *IEEE Transactions on Power Apparatus and Systems*, vol. PAS-91, no. 5, pp. 1848–1854, Sep. 1972, ISSN: 0018-9510. DOI: 10.1109/TPAS.1972.293509.
- [12] A. Ahmadi, S. Mahbubi, and M. Shahnazari, "Rotating rectifier fault detection in brushless excitation system of synchronous generators," en, in *2019 27th Iranian Conference on Electrical Engineering (ICEE)*, Yazd, Iran: IEEE, Apr. 2019, pp. 1–5, ISBN: 978-1-72811-508-5. DOI: 10.1109/IranianCEE.2019.8822368.
- [13] B. M. Weedy, B. J. Cory, N. Jenkins, J. B. Ekanayake, and G. Strbac, *Electric Power Systems*, en. John Wiley & Sons, Jul. 2012, ISBN: 978-1-118-36108-5.
- [14] "IEEE Guide for Synchronous Generator Modeling Practices and Parameter Verification with Applications in Power System Stability Analyses," en, IEEE, Tech. Rep. DOI: 10.1109/IEEESTD.2020.9020274.
- [15] R. H. Park, "Two-reaction theory of synchronous machines generalized method of analysis-part I," en, p. 12, 1929.
- [16] ———, "Two-reaction theory of synchronous machines-II," en, *Transactions of the American Institute of Electrical Engineers*, vol. 52, no. 2, pp. 352–354, Jun. 1933, ISSN: 0096-3860. DOI: 10.1109/T-AIEE.1933.5056309.
- [17] P. Vernekar, Z. Wang, A. Serrani, and K. Passino, "Feedback Control Methods for a Single Machine Infinite Bus System," en, p. 144,
- [18] M. Basler, "Excitation systems: The current state of the art," en, in *2006 IEEE Power Engineering Society General Meeting*, Montreal, Que., Canada: IEEE, 2006, 7 pp. ISBN: 978-1-4244-0493-3. DOI: 10.1109/PES.2006.1709610.
- [19] M. Kumar Sharma, R. Pathak, M. Kumar Jha, and M. Qureshi, "Excitation control of a power plant alternator using interval type-2 fuzzy logic controller," en, *Advances in Modelling and Analysis C*, vol. 73, no. 4, pp. 182–188, Dec. 2018, ISSN: 12404535. DOI: 10.18280/ama_c.730407.
- [20] A. Vahedi, "Rotary diode failure detection in brushless exciter system of power plant synchronous generator," en, in *2016 6th Conference on Thermal Power Plants (CTPP)*, Tehran, Iran: IEEE, Jan. 2016, pp. 6–11, ISBN: 978-1-5090-0372-3. DOI: 10.1109/CTPP.2016.7482926.
- [21] J. R. Williams, "The amplidyne," en, *Electrical Engineering*, vol. 65, no. 5, pp. 208–213, May 1946, ISSN: 0095-9197. DOI: 10.1109/EE.1946.6441670.
- [22] N. Mohan, T. M. Undeland, and W. P. Robbins, *Power Electronics: Converters, Applications, and Design*, en, 3rd ed. Hoboken, NJ: John Wiley & Sons, 2003, ISBN: 978-0-471-22693-2.
- [23] L. Sivertsen, *Elektriske Maskiner*, no. 1. Vigmostad & Bjørke AS, Jul. 2019.

- [24] E. Irmak, N. Guler, and M. Ersan, "PI controlled solar energy supported static excitation system desing and simulation for synchronous generators," in *2016 IEEE International Conference on Renewable Energy Research and Applications (ICRERA)*, Birmingham, United Kingdom: IEEE, Nov. 2016, pp. 1024–1028, ISBN: 978-1-5090-3388-1. DOI: 10.1109/ICRERA.2016.7884489.
- [25] A. Mansoor, W. Grady, R. Thallam, M. Doyle, S. Krein, and M. Samotyj, "Effect of supply voltage harmonics on the input current of single-phase diode bridge rectifier loads," en, *IEEE Transactions on Power Delivery*, vol. 10, no. 3, pp. 1416–1422, Jul. 1995, ISSN: 08858977. DOI: 10.1109/61.400924.
- [26] G. V. Aparna, G. Suresh Babu, and T. M. Krishna, "Simulation and Analysis of Single Phase Full Bridge Diode Rectifier with Different Passive Power Factor Correction Techniques," en, in *2018 International Conference on Recent Innovations in Electrical, Electronics & Communication Engineering (ICRIEECE)*, Bhubaneswar, India: IEEE, Jul. 2018, pp. 2351–2355, ISBN: 978-1-5386-5995-3. DOI: 10.1109/ICRIEECE44171.2018.9008888.
- [27] S.-I. Motegi and Y. Nishida, "Three-Phase PFC Rectifier by Means of Three Single-Phase Passive PFC Units," en, in *2019 10th International Conference on Power Electronics and ECCE Asia (ICPE 2019 - ECCE Asia)*, Busan, Korea (South): IEEE, May 2019, pp. 829–832, ISBN: 978-89-5708-313-0. DOI: 10.23919/ICPE2019-ECCEAsia42246.2019.8797054.
- [28] Z. Meng-di, W. Xi-xiu, Q. Wei, L. Fei, and L. Bo, "Application of PID control based on BP-NN for marine generator excitation system," en, in *2012 Power Engineering and Automation Conference*, Wuhan, Hubei, China: IEEE, Sep. 2012, pp. 1–4, ISBN: 978-1-4577-1600-3 978-1-4577-1599-0. DOI: 10.1109/PEAM.2012.6612457.
- [29] Y. Cao and J. Ma, "Research on PID parameters optimization of synchronous generator excitation control system," en, in *2010 5th International Conference on Critical Infrastructure (CRIS)*, Beijing, China: IEEE, Sep. 2010, pp. 1–5, ISBN: 978-1-4244-8080-7. DOI: 10.1109/CRIS.2010.5617581.
- [30] S. Yuqiu, Z. Jibin, and S. Jianxin, "The Analysis and Simulation of Closed-loop Paper Tension Control System Based on MATLAB in the Web Offset," en, in *2012 Third International Conference on Digital Manufacturing & Automation*, Guilin, China: IEEE, Jul. 2012, pp. 881–883, ISBN: 978-1-4673-2217-1 978-0-7695-4772-5. DOI: 10.1109/ICDMA.2012.207.
- [31] R. A. Hyde, "Using Simscape™ to Support System-Level Design," en, p. 6,
- [32] "Simscape Electrical Reference (Specialized Power Systems)," en, p. 980,
- [33] T. Fischer, "Terminal Voltage and Reactive Power Control of a Synchronous Generator Through Transmission Lines," en, p. 127,

- [34] P. Dedie, V. Brommer, and S. Scharnholz, "ICCOS Countercurrent-Thyristor High-Power Opening Switch for Currents Up to 28 kA," en, *IEEE Transactions on Magnetics*, vol. 45, no. 1, pp. 536–539, Jan. 2009, ISSN: 0018-9464. DOI: 10.1109/TMAG.2008.2008428.

Appendices

A Park transformation

\mathbf{P} shows the matrix for the park transformation, that transforms the stator variables into rotor variables. These steps are shown in equation A.1, A.2, A.3 and A.4.

$$\mathbf{P} = \sqrt{\frac{2}{3}} \begin{bmatrix} \frac{1}{\sqrt{3}} & \frac{1}{\sqrt{3}} & \frac{1}{\sqrt{3}} \\ \cos\theta & \cos(\theta - \frac{2\pi}{3}) & \cos(\theta + \frac{2\pi}{3}) \\ \sin\theta & \sin(\theta - \frac{2\pi}{3}) & \sin(\theta + \frac{2\pi}{3}) \end{bmatrix} \quad (\text{A.1})$$

$$\mathbf{P}^{-1} = \mathbf{P}^T = \sqrt{\frac{2}{3}} \begin{bmatrix} \frac{1}{\sqrt{2}} & \cos\theta & \sin\theta \\ \frac{1}{\sqrt{2}} & \cos(\theta - \frac{2\pi}{3}) & \sin(\theta - \frac{2\pi}{3}) \\ \frac{1}{\sqrt{2}} & \cos(\theta + \frac{2\pi}{3}) & \sin(\theta + \frac{2\pi}{3}) \end{bmatrix} \quad (\text{A.2})$$

$$\mathbf{P}^{-1} \triangleq \begin{bmatrix} \mathbf{P} & \mathbf{0} \\ \mathbf{0} & \mathbf{1} \end{bmatrix}, \quad \mathbf{B}^{-1} = \mathbf{B}^T = \begin{bmatrix} \mathbf{P}^T & \mathbf{0} \\ \mathbf{0} & \mathbf{1} \end{bmatrix} \quad (\text{A.3})$$

$$\mathbf{v}_B \triangleq \mathbf{B}\mathbf{v}, \quad \mathbf{i}_B \triangleq \mathbf{B}\mathbf{i}, \quad \boldsymbol{\lambda}_B \triangleq \mathbf{B}\boldsymbol{\lambda} \quad (\text{A.4})$$

The time various expressions for the stator and exciter coil, quadrature and direct axis inductances. All of these are variouse by the placement of the rotor, and the placement is given by θ . [1]

$$L_{aa} = \frac{\lambda_{aa'}}{i_a} = L_s + L_m \cos(2\theta) \quad (\text{A.5})$$

$$L_{bb} = \frac{\lambda_{bb'}}{i_b} = L_s + L_m \cos(2\theta - \frac{2\pi}{3}) \quad (\text{A.6})$$

$$L_{cc} = \frac{\lambda_{cc'}}{i_c} = L_s + L_m \cos(2\theta + \frac{2\pi}{3}) \quad (\text{A.7})$$

$$L_{ab} = L_{ba} = \frac{\lambda_{aa'}}{i_b} = -[M_s + L_m \cos 2(\theta + \frac{\pi}{6})] \quad (\text{A.8})$$

$$L_{bc} = L_{cb} = \frac{\lambda_{bb'}}{i_c} = -[M_s + L_m \cos 2(\theta + \frac{\pi}{2})] \quad (\text{A.9})$$

$$L_{ca} = L_{ac} = \frac{\lambda_{cc'}}{i_a} = -[M_s + L_m \cos 2(\theta + \frac{5\pi}{6})] \quad (\text{A.10})$$

$$L_{aD} = L_{Da} = M_D \cos \theta \quad (\text{A.11})$$

$$L_{bD} = L_{Db} = M_D \cos(\theta - \frac{2\pi}{3}) \quad (\text{A.12})$$

$$L_{cD} = L_{Dc} = M_D \cos(\theta + \frac{2\pi}{3}) \quad (\text{A.13})$$

$$L_{aF} = L_{Fa} = M_F \cos \theta \quad (\text{A.14})$$

$$L_{bF} = L_{Fb} = M_F \cos(\theta - \frac{2\pi}{3}) \quad (\text{A.15})$$

$$L_{cF} = L_{Fc} = M_F \cos(\theta + \frac{2\pi}{3}) \quad (\text{A.16})$$

$$L_{aQ} = L_{Qa} = M_Q \cos \theta \quad (\text{A.17})$$

$$L_{bQ} = L_{Qb} = M_Q \cos(\theta - \frac{2\pi}{3}) \quad (\text{A.18})$$

$$L_{cQ} = L_{Qc} = M_Q \cos(\theta + \frac{2\pi}{3}) \quad (\text{A.19})$$

$$L_{DF} = L_{FD} = M_R, \quad L_{FQ} = L_{QF} = 0, \quad L_{DQ} = L_{QD} = 0 \quad (\text{A.20})$$

$$L_{DD} = L_Q, \quad L_F = L_F, \quad L_{QQ} = L_Q \quad (\text{A.21})$$

Expressions for the transformed voltages, fluxes and inductances for the park transformation. The zero sequence is given by equation A.22. [1]

$$v_0 = -r i_0 - \frac{d\alpha_0}{dt} \quad (\text{A.22})$$

The direct axis equations are given in equations A.23, A.24 and A.25.

$$v_0 = -r i_d - \frac{d\theta}{dt} \alpha_q - \frac{d\alpha_d}{dt} \quad (\text{A.23})$$

$$v_F = r_F i_F + \frac{d\alpha_F}{dt} \quad (\text{A.24})$$

$$v_D = r_D i_D + \frac{d\alpha_D}{dt} = 0 \quad (\text{A.25})$$

The quadrature axis equations are given in equations A.26 and A.27.

$$v_q = -r i_q - \frac{d\theta}{dt} \alpha_d - \frac{d\alpha_q}{dt} \quad (\text{A.26})$$

$$v_Q = -r_Q i_Q + \frac{d\alpha_Q}{dt} = 0 \quad (\text{A.27})$$

$$L_0 = L_s - 2M_s \quad (\text{A.28})$$

$$L_d = L_s + M_s + \frac{3}{2}L_m \quad (\text{A.29})$$

$$L_q = L_s + M_s - \frac{3}{2}L_m \quad (\text{A.30})$$

B Simulink Model

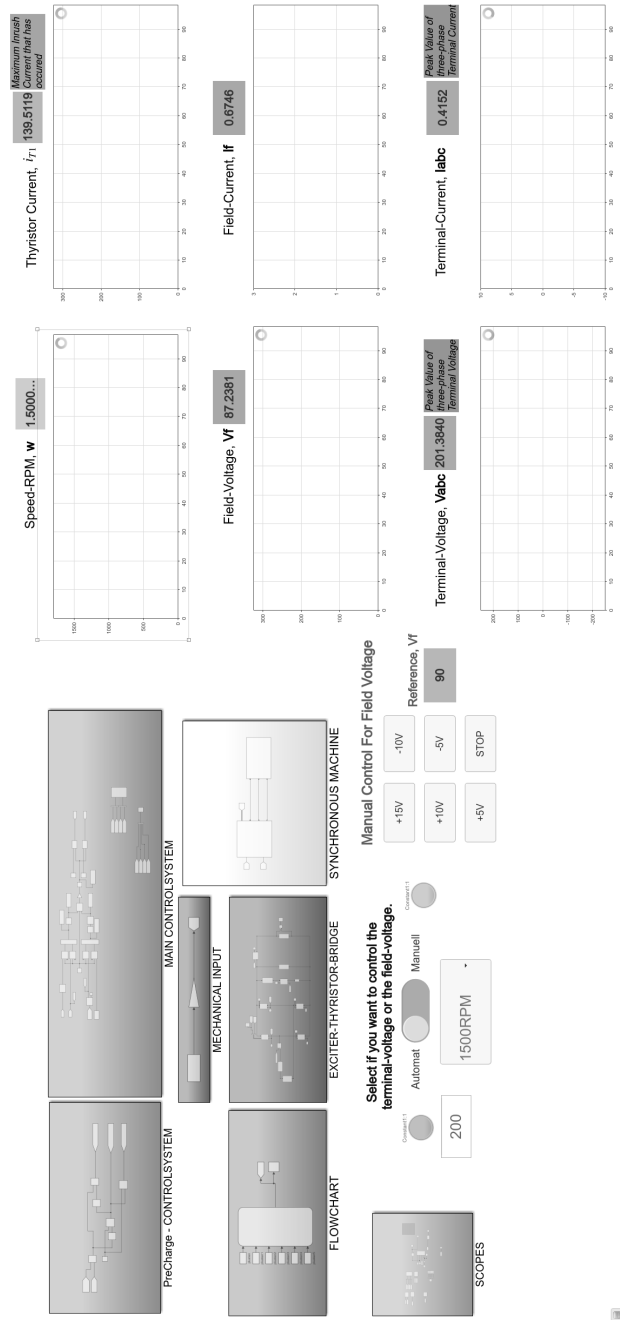


Figure B.1: Full Simulink Model.

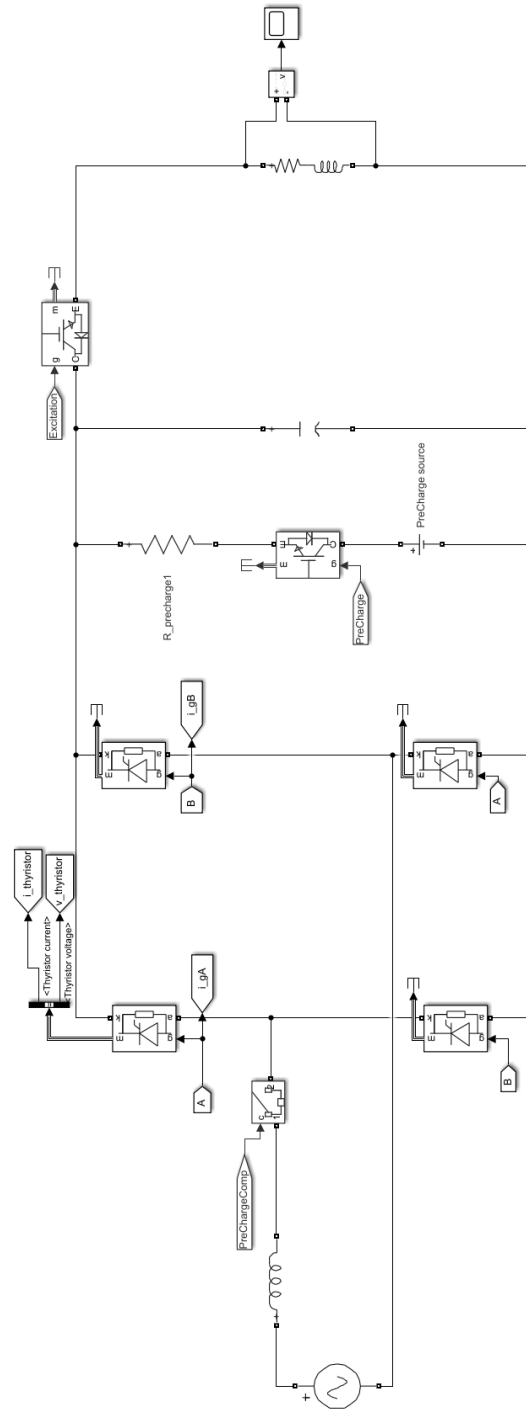


Figure B.3: Thyristor Bridge

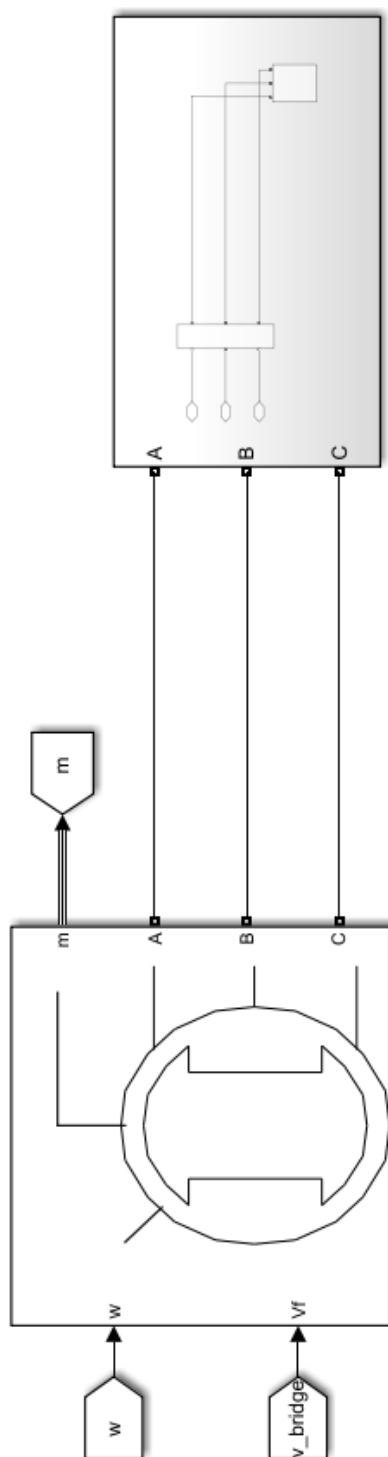


Figure B.4: Synchronous Machine connected to load

C Ziegler-Nichols & Cohen-Coon Tuning

Table C.1 and C.2 shows the equations for calculating the P, I and D for Ziegler-Nichols and Cohen-Coon, respectively.

	K_P	T_r	T_d
P	$\frac{\nu_0}{K_0\tau_0}$		
PI	$\frac{0.9\nu_0}{K_0\tau_0}$	$3\tau_0$	
PID	$\frac{1.2\nu_0}{K_0\tau_0}$	$2\tau_0$	$0.5\tau_0$

Table C.1: Ziegler-Nichols tuning by using reaction curve.

	K_P	T_r	T_d
P	$\frac{\nu_0}{K_0\tau_0}$		
PI	$\frac{\nu_0}{K_0\tau_0} \left[0.9 + \frac{\tau_0}{12\nu_0} \right]$	$\frac{30\nu_0 + 3\tau_0}{9\nu_0 + 20\tau_0}$	
PID	$\frac{\nu_0}{K_0\tau_0} \left[\frac{4}{3} + \frac{\tau_0}{4\nu_0} \right]$	$\frac{\tau_0 [32\nu_0 + 6\tau_0]}{13\nu_0 + 8\tau_0}$	$\frac{4\tau_0\nu_0}{11\nu_0 + 2\tau_0}$

Table C.2: Cohen-Coon tuning by using reaction curve.

D General

D.1 Terco MV1027-235

The SM that the simulated machine is suppose to behave like is a Terco MV1027-235 with serial number: 39333. This machine consists of two damper windings and all parameters from the datasheet are listed in table D.1.

Technical Specifications	Datasheet	Name plate
$Power_{Generator}$	1.2 kVA	1.2 kVA
$\cos\phi$	0.8	0.8
$Power_{Motor}$	1.0 kW	1.0 kW
$Voltage_{Star}$	220 – 240 V	220 – 240 V
$Current_{Star}$	3.5 A	3.5 A
$Voltage_{Delta}$	127 – 140 V	220 – 240 V
$Current_{Delta}$	6.1 A	3.5 A
$DC_{ExcitationVoltage}$	220 V	220 V
$DC_{ExcitationCurrent}$	1.4 A	1.4 A
Temp.Class		F(155·)
Protection		IP23
Duty Type		S260min
Norm		EN60034 : 1993

Table D.1: Parameters for Terco MV1027-235.

D.2 Littelfuse S6065KTP

The SM that the simulated machine is suppose to behave like is a Terco MV1027-235 with serial number: 39333. This machine consists of two damper windings and all parameters from the datasheet are listed in table D.2.

Table D.2: Parameters for Thyristor/SCR.

Technical Specifications	Datasheet
Rated Average On-State Current	65 A
Thyristor Type	SCR
Package Type	TO-218AC
Repetitive Peak Reverse Voltage	600 V
Surge Current Rating	950A
Mounting Type	Through Hole
Maximum Gate Trigger Current	50 mA
Maximum Gate Trigger Voltage	2 V
Maximum Holding Current	80 mA
Pin Count	3
Dimensions	16x4.78x21.21 mm
Peak On-State Voltage	1.8 V
Minimum Operating Temperature	-40° C
Maximum Operating Temperature	+125° C
Repetitive Peak Off-State Current	0.02 mA

D.3 Component List

A component list has been made in table D.3, for future students.

Table D.3: Parameters for Terco MV1027-235.

System Part	Component	Quantity	Manufacturer Name	Specification
AC/DC Stage	S6065KTP	4	Littelfuse	65A, 600V
AC/DC Stage	Capacitor	1	ALS70H273QW250	27000 μ F, 250V
AC/DC Stage	Resistor	1	TE500B100RJ	100 Ω , 500W W
Precharge Circuit	IGBT	3	STGF20H60DF	40A, 600V
Basic	Current Sensor	2	LEM LAH 50-P	0 – 50 A
Basic	Voltage Sensor	3	LEM LV 25-P	10 – 500 V

Index

- AC Excitation System (Type AC), 11–15, 17, 48, 51
- Alternating Current (AC), 4, 11–19, 27, 28, 30, 48, 49, 51
- Automatic Power Factor Regulator (APFR), vi, 19, 20
- Automatic Reactive Power Regulator (AQR), vi, viii, 19, 20
- Automatic Voltage Regulator (AVR), 4, 11, 20, 21
- DC Excitation System (Type DC), 11, 12
- Differential (D), vi, XII, 24
- Direct Current (DC), 2, 4, 5, 11–17, 19, 27–29, 34, 40, 48, 51
- Electromotive Force (EMF), 6
- Institute of Electrical and Electronics Engineers (IEEE), 2, 11
- Integral (I), vi, XII, 24, 32, 33, 37
- Over-excitation Limiter (OEL), vi, 22
- Permanent Magnet Synchronous Generator (PMSG), 14
- Power System Stabilizer (PSS), vi, 22, 23
- Proportional (P), vi, XII, 23, 32, 33, 37
- Proportional Differential (PD), 23, 25
- Proportional Integral (PI), XII, 23, 25, 26, 32, 33, 36, 47–50
- Proportional Integral Differential (PID), viii, XII, 4, 11, 23, 25, 26
- Root Mean Square (RMS), 28, 30, 38
- Rotations per Minute (RPM), ix, 5, 38, 39, 45, 46, 49
- Semiconductor Controlled Rectifiers (SCR), vi, ix, x, XIV, 27–35, 40, 43–45, 47–51
- Static Excitation System (Type ST), 12, 15, 17
- Synchronous Machine (SM), viii, x, XIII, 2, 4–9, 11–15, 27–30, 33, 48, 49, 51
- Under-excitation Limiter (UEL), vi, 21, 22